Available online at www.sciencedirect.com
ScienceDirect
Nuclear Physics B 796 (2008) 137–183
NUCLEAR PHYSICS B
www.elsevier.com/locate/nuclphysb

Resummation of hadroproduction cross-sections at high energy

Richard D. Ball

School of Physics, University of Edinburgh, JCMB, KB, Mayfield Rd, Edinburgh EH9 3JZ, Scotland, UK
CERN, Department of Physics, Theory Division, CH-1211 Genève 23, Switzerland

Received 9 August 2007; received in revised form 2 December 2007; accepted 4 December 2007

Available online 23 December 2007

Abstract

We reconsider the high energy resummation of photoproduction, electroproduction and hadroproduction cross-sections, in the light of recent progress in the resummation of perturbative parton evolution to NLO in logarithms of Q^2 and x. We show in particular that the when the coupling runs the dramatic enhancements seen at fixed coupling, due to infrared singularities in the partonic cross-sections, are substantially reduced, to the extent that they are largely accounted for by the usual NLO and NNLO perturbative corrections. This leads to a novel explanation of the large K-factors commonly found in perturbative calculations of hadroproduction cross-sections. We give numerical estimates of high energy resummation effects for inclusive B-production, inclusive jets, Drell–Yan and vector boson production, along with their rapidity distributions. We find that resummation modifies the B-production cross-section at the LHC by at most 15%, but that the enhancement of gluonic W-production may be as large as 50% at large rapidities.

PACS: 12.38.Cy; 13.85.Ni; 13.85.Qk

Keywords: Perturbative QCD; High energy resummation; Hadroproduction

1. Introduction

At the LHC we hope to separate with confidence a tiny fraction of interesting events from an overwhelming background of collisions involving gluons carrying only a small fraction of the momentum in the beams. The success of this enterprise depends crucially on our ability to control

E-mail addresses: rdb@ph.ed.ac.uk, rball@cern.ch.

0550-3213/$ – see front matter
doi:10.1016/j.nuclphysb.2007.12.014

high energy logarithms in perturbative QCD at leading twist when we calculate inclusive cross-sections. Currently however no reliable calculations of high energy resummation corrections to any hadronic process have been made. The purpose of this paper is to remove the one remaining obstacle to performing such calculations.

In recent years there has been considerable progress by several groups in understanding the resummation of parton evolution, so that we now know how to simultaneously resum all collinear and small-x logarithms at NLO. This programme depended on several key ingredients: k_T-factorisation [1,2], NLLx corrections [3–5], the recognition of the need to simultaneously resum collinear, anti-collinear and high energy logarithms [6,7], the use of high energy duality to achieve this [8,9], and the understanding of running coupling effects [10–13]. It is now possible to perform precise and reliable calculations of small-x resummation corrections to parton distribution functions.

Hadroproduction processes have received much less attention [14–17]. The reason for this is partly their additional kinematic complexity, but also because of a difficult conceptual problem standing in the way of reliable results. This problem relates to the infrared singularity which appears when two gluons collide at high energy, due to the possibility of all the energy going into a timelike gluon which may then go almost on-shell [15]. Though it has been understood for some time that this singularity might produce substantial enhancements of hadronic cross-sections, it has been difficult to make reliable predictions, particularly when the coupling runs [16]. This is the problem we resolve in this paper. We will find that the singularity is less dangerous than naive arguments suggest, that the enhancements it produces at high energy are modest, and in fact may be well approximated by the NLO and NNLO perturbative results.

The structure of the rest of the paper is as follows: in Section 2 we summarise the main ideas used in the resummation of high energy logarithms in order to set the scene and fix notation, and then explain the difficulties encountered in applying these ideas to the resummation of hadronic cross-sections due to infrared singularities. In Section 3 we consider the simpler scenario of photoproduction and electroproduction processes, and in particular how there infrared singularities may be dealt with using an exponentiation trick. We apply this trick to the inclusive photoproduction of $b\bar{b}$-pairs, providing quantitative estimates of resummation effects. We then in Section 4 move on to the more interesting case of hadroproduction, construct the gluon–gluon luminosity, describe the singularity structure of the partonic cross-sections, and show how the same trick used in photoproduction works here also. We provide generic estimates for resummation effects in various hadroproduction processes at the Tevatron, LHC and a notional VLHC, and consider in detail the particular case of hadroproduction of $b\bar{b}$ pairs. We also consider the stability of the resummed perturbative expansion. In Section 5 we consider how we may compute rapidity distributions in this framework, and offer estimates of resummation corrections for the rapidity distributions of $b\bar{b}$ pairs and W bosons at LHC. Finally in Section 6 we summarise our results, and suggest several directions for future work.

2. High energy singularities

2.1. High energy factorization

We consider electron–hadron, photon–hadron and hadron–hadron processes in which Q is the hard (transverse) scale (for example the photon virtuality, a heavy quark mass, or the invariant mass of some particular particles in the final state), S the square of the centre-of-mass energy, and $\rho \equiv Q^2/S$. The dimensionless cross-section $\Sigma \equiv Q^2\sigma$ is a function of ρ and Q, the scale of

Q being set by $\Lambda_{\rm QCD}$. For hard processes $Q \gg \Lambda_{\rm QCD}$, while for high energy processes $S \gg Q^2$, so $\rho \ll 1$.

In an electroproduction or photoproduction process, if x and $\mathbf{k}$ are the longitudinal and transverse momenta of the struck parton, the square of the centre-of-mass energy of the hard process is $s = xS$, and the dimensionless hard cross-section $\Sigma_{\gamma j} \equiv Q^2\sigma_{\gamma j}$ is a function of $Q^2/s = \rho/x$, $\mathbf{k}/Q$ and μ/Q, where μ is the factorization and renormalization scale (here set equal), and j labels the struck parton. The (unintegrated) parton distribution function $\mathcal{F}_j$ depends only on x, $\mathbf{k}^2$ and μ^2. Factorization (or more specifically "k_T-factorization" [1,2,14,15]) is then the statement that the photon–hadron cross-section may be written as

$$\Sigma_{\gamma\rm h}(\rho, Q) = \sum_{j=g,q,\bar{q}} \int_\rho^1 \frac{dx}{x} \int \frac{d^2\mathbf{k}}{\pi\mathbf{k}^2} \Sigma_{\gamma j}\left(\frac{\rho}{x}, \frac{\mathbf{k}}{Q}, \alpha_s\big(\mu^2\big)\right) \mathcal{F}_j\big(x, \mathbf{k}^2, \mu^2\big), \tag{2.1}$$

up to terms which vanish as inverse powers of the hard scale Q.

For a purely hadronic process, the centre-of-mass energy of the hard process is $s = x_1x_2S$, where x_1 and x_2 are the longitudinal momentum fractions of the colliding partons j_1 and j_2 in hadrons h_1 and h_2. The dimensionless hard cross-section $\Sigma_{j_1j_2} \equiv Q^2\sigma_{j_1j_2}$ is then a function of $Q^2/s = \rho/x_1x_2$, $\mathbf{k}_1/Q$, $\mathbf{k}_2/Q$ and μ/Q, so factorization is the statement that the hadron–hadron cross-section may be written as

$$\begin{aligned}\Sigma_{\rm hh}(\rho, Q) = \sum_{j_1,j_2=g,q,\bar{q}} &\int_\rho^1 \frac{dx_1}{x_1} \int_\rho^1 \frac{dx_2}{x_2} \int \frac{d^2\mathbf{k}_1}{\pi\mathbf{k}_1^2} \int \frac{d^2\mathbf{k}_2}{\pi\mathbf{k}_2^2} \\ &\times \Sigma_{j_1j_2}\left(\frac{\rho}{x_1x_2}, \frac{\mathbf{k}_1}{Q}, \frac{\mathbf{k}_2}{Q}, \alpha_s\big(\mu^2\big)\right) \mathcal{F}_{j_1}\big(x_1, \mathbf{k}_1^2, \mu^2\big) \mathcal{F}_{j_2}\big(x_2, \mathbf{k}_2^2, \mu^2\big),\end{aligned} \tag{2.2}$$

again up to terms which vanish as inverse powers of the hard scale Q. The dependence on μ will be suppressed in what follows: in practice we will take $\mu = Q$.

2.2. Gluon dominance at high energy

The range of x and Q relevant at lepton–hadron and hadron–hadron colliders (specifically HERA with $\sqrt{S} = 320$ GeV, the Tevatron with $\sqrt{S} = 1.8$ TeV, the LHC with $\sqrt{S} = 14$ TeV and a notional VLHC with $\sqrt{S} = 200$ TeV) is shown in Fig. 1. It is obvious from the figure that over most of the kinematic reach of these machines x is small, and thus small x logarithms are potentially large: only for processes at the highest scales (for which the cross-sections are correspondingly small) can the small x region be altogether excluded.

High energy processes thus usually involve collisions of small x partons, and at small x and high Q^2 it is now well known that all singlet parton distributions show a steep rise, that of the gluon distribution $G(x, Q^2)$ being driven by the non-Abelian splitting $g \to gg$, and that of the singlet quark distribution $Q(x, Q^2)$ by $g \to q\bar{q}$ [18,19]. Because the latter process is $O(\alpha_s)$, at small x and high Q^2 the singlet quark distribution is always smaller by a power of $\alpha_s(Q^2)$ than the gluon, i.e. $Q(x, Q^2) \simeq \alpha_s(Q^2)G(x, Q^2)$: at small x most partons are gluons.

This means that when we compute high energy partonic cross-sections we can no longer rely on the simple counting of powers of α_s as we do when Q and S are comparable. Consider for example a Drell–Yan type of process: formally the LO process is $q\bar{q}$ annihilation, Fig. 2(a), and is $O(\alpha)$, while the qg (and $\bar{q}g$) scattering processes Fig. 2(b) and (c) are both NLO, i.e. $O(\alpha\alpha_s)$,

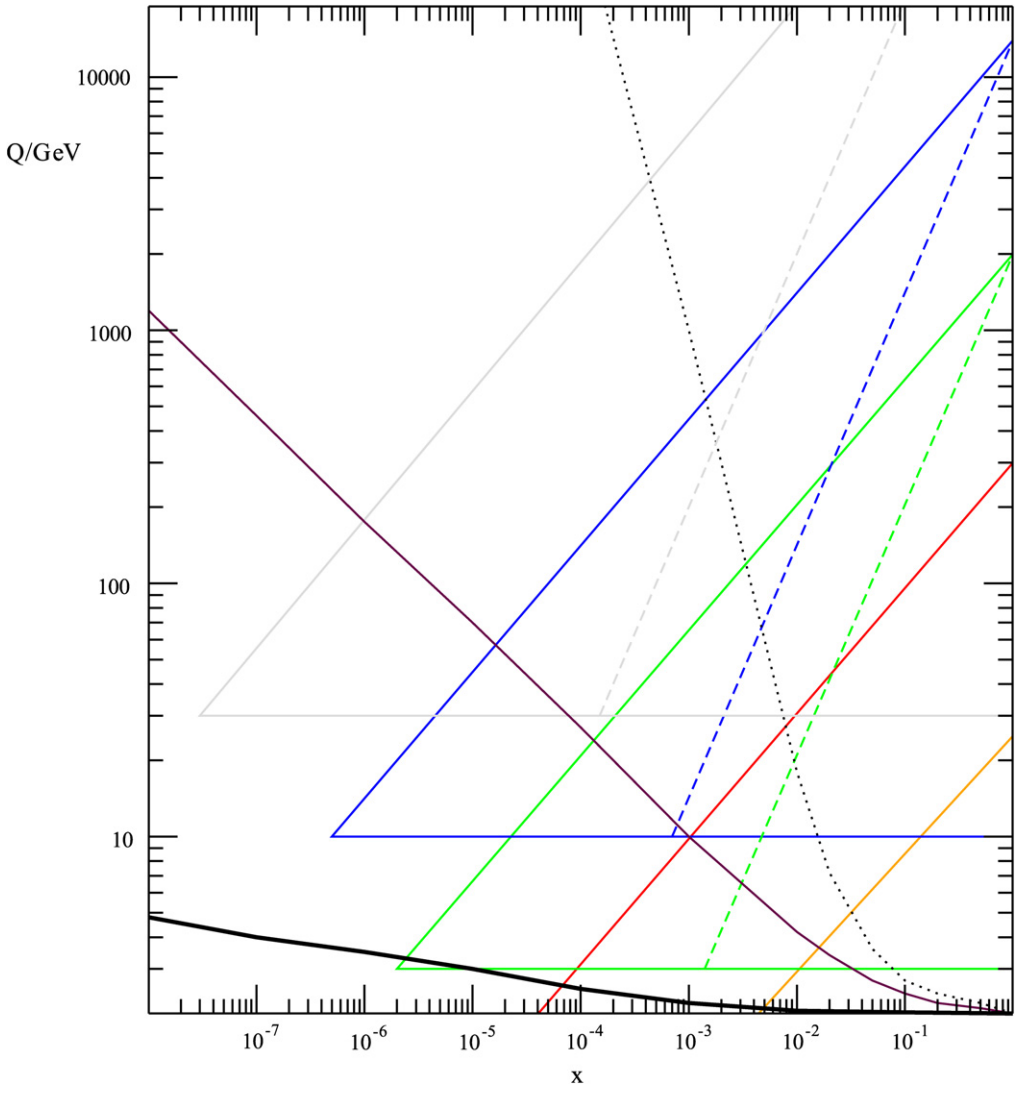

Fig. 1. The kinematic plane for electron–hadron and hadron–hadron collisions: x is the fraction of longitudinal momentum in the parton, and Q is the hard scale in GeV (which for photoproduction and hadroproduction is the invariant mass of the particles produced in the hard process). Shown are the regions accessible in fixed target experiments (orange), at HERA (red), at the Tevatron (green), at LHC (blue) and at a notional VLHC with $S = 200$ TeV (grey). The dashed lines for the hadron colliders show the central rapidity region, where $x_1 = x_2 = x$: when the rapidity is nonzero, the values of x_1 and x_2 may be read off for a given Q by choosing points symmetrically placed about this line. The solid black diagonal line shows the points at which $\dot{L}_z = L'_z$, and thus the logarithms of Q^2 are as important as the logarithms of x (see Eq. (6.1)): the dotted black line is determined by $\dot{L}_z = 0.1L'_z$, while the heavy black line is determined by $\dot{L}_z = 10L'_z$. (For interpretation of the references to colour in this figure legend, the reader is referred to the web version of this article.)

and the gg processes Fig. 3 are all $O(\alpha\alpha_s^2)$ and thus NNLO. However at high energy, if we take into account the relative suppression of the quark relative to the gluon, all of these contributions are in practice $O(\alpha\alpha_s^2)$, and thus should be considered as leading order. Subleading contributions

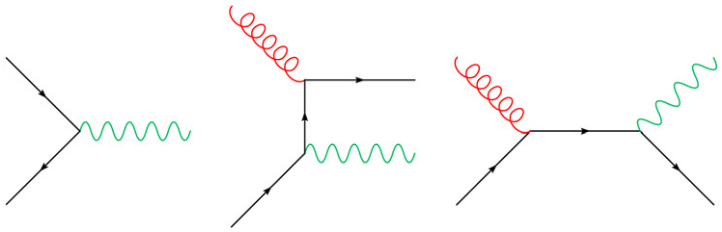

Fig. 2. The quark induced Drell–Yan process, or vector boson production (a) the $O(\alpha)$ $q\bar{q}$ annihilation process and (b), (c) the $O(\alpha\alpha_s)$ qg (or $\bar{q}g$) fusion process, with initial and final state radiation respectively.

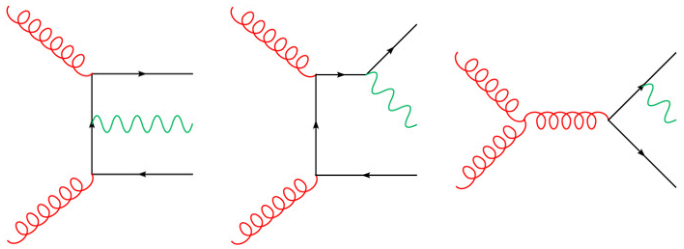

Fig. 3. The gluon induced Drell–Yan process, or vector boson production: the three main classes of contribution (a) with initial state radiation, (b) with both initial and final state radiation and (c) with final state radiation only. All these processes are formally $O(\alpha\alpha_s^2)$.

to the $q\bar{q}$ and qg contributions in Fig. 2 are known [20]: the subleading contributions to the gg processes Fig. 3 are not known at present, since formally they would be NNNLO.

In this paper we shall only consider processes with gluons in the initial state. In practice this means that we simply drop the summation over partons in Eqs. (2.1), (2.2). This simplification is sufficient to discuss most of the issues in high energy resummation, but will of necessity mean that our numerical results are estimates rather than calculations of complete cross-sections.

2.3. Double Mellin transforms

The convolutions over x and $\mathbf{k}$ in the factorizations (2.1) and (2.2) may be undone by taking Mellin transforms with respect to ρ and Q. Explicitly if we define

$$\Sigma_{\gamma h}(N,M)=\int_0^1\frac{d\rho}{\rho}\rho^N\int_0^\infty\frac{dQ^2}{Q^2}\left(\frac{Q^2}{\Lambda^2}\right)^{-M}\Sigma_{\gamma h}\left(\rho,Q^2\right), \tag{2.3}$$

while for the hard cross-section

$$\mathcal{C}(N,M)=\int_0^1\frac{d\rho}{\rho}\rho^N\int\frac{d^2\mathbf{k}}{\pi\mathbf{k}^2}\left(\frac{\mathbf{k}^2}{Q^2}\right)^M\Sigma_{\gamma g}\left(\rho,\frac{\mathbf{k}}{Q}\right), \tag{2.4}$$

then if the double Mellin transform of the unintegrated gluon distribution $\mathcal{G} \equiv \mathcal{F}_g$ is

$$\mathcal{G}(N,M) = \int_0^1 \frac{dx}{x} x^N \int_0^\infty \frac{dk^2}{k^2} \left(\frac{k^2}{\Lambda^2}\right)^{-M} \mathcal{G}\left(x,k^2\right), \tag{2.5}$$

the factorization (2.1) becomes simply algebraic: the purely gluonic contribution to the transformed cross-section is

$$\Sigma_{\gamma \mathrm{h}}(N,M) = \mathcal{C}(N,M)\mathcal{G}(N,M). \tag{2.6}$$

It is easier to make contact with phenomenology if instead of working with the unintegrated gluon distribution we define the integrated distribution

$$G\left(x,Q^2\right) = \int_0^{Q^2} \frac{dk^2}{k^2} \mathcal{G}\left(x,k^2\right). \tag{2.7}$$

This is the distribution that would be proportional to the physical cross-section if the hard process were pointlike, i.e. the hard cross-section was simply proportional to $\Theta(Q^2-k^2)$. Then in Mellin space

$$G(N,M) = M^{-1}\mathcal{G}(N,M), \tag{2.8}$$

and Eq. (2.6) becomes

$$\Sigma_{\gamma \mathrm{h}}(N,M) = C(N,M)G(N,M), \tag{2.9}$$

where $C(N,M) \equiv M\mathcal{C}(N,M)$.

To recover the physical cross-section we invert the two Mellin transforms (2.3):

$$\Sigma_{\gamma \mathrm{h}}(\rho,Q) = \int_{-i\infty}^{i\infty} \frac{dN}{2\pi i} e^{\xi N} \int_{-i\infty}^{i\infty} \frac{dM}{2\pi i} e^{tM} C(N,M)G(N,M), \tag{2.10}$$

where for clarity in future discussions we have defined

$$\xi \equiv \log 1/\rho, \qquad t \equiv \log Q^2/\Lambda^2. \tag{2.11}$$

Here N and M are both complex variables: the contours in the integrations over N and M keep just to the right of the singularities near $N=0$ and $M=0$. The contour in N is always closed on the left (since $\xi > 0$): the contour in M is closed on the left in the ultraviolet ($t > 0$), but on the right in the infrared ($t < 0$).

For hadronic processes we proceed similarly: defining

$$\mathcal{H}(N,M_1,M_2) = \int_0^1 \frac{d\rho}{\rho} \rho^N \int \frac{d^2\mathbf{k}_1}{\pi \mathbf{k}_1^2} \left(\frac{\mathbf{k}_1^2}{Q^2}\right)^{M_1} \int \frac{d^2\mathbf{k}_2}{\pi \mathbf{k}_2^2} \left(\frac{\mathbf{k}_2^2}{Q^2}\right)^{M_2} \Sigma_{gg}\left(\rho, \frac{\mathbf{k}_1}{Q}, \frac{\mathbf{k}_2}{Q}\right), \tag{2.12}$$

the factorization formula (2.2) becomes

$$\Sigma_{\mathrm{hh}}(N,M_1,M_2) = H(N,M_1,M_2)G(N,M_1)G(N,M_2), \tag{2.13}$$

where $H(N, M_1, M_2) = M_1 M_2 \mathcal{H}(N, M_1, M_2)$. The hadronic cross-section is thus

$$\Sigma_{\rm hh}(\rho, Q) = \int_{-i\infty}^{i\infty} \frac{dN}{2\pi i} e^{\xi N} \int_{-i\infty}^{i\infty} \frac{dM_1}{2\pi i} \frac{dM_2}{2\pi i} e^{t(M_1+M_2)} \times H(N, M_1, M_2) G(N, M_1) G(N, M_2), \tag{2.14}$$

and we have to deal with functions of the three complex variables N, M_1 and M_2 integrated along three contours. Clearly $H(N, M_1, M_2) = H(N, M_2, M_1)$.

2.4. Duality at fixed coupling

Perturbative expansions of the hard cross sections are contaminated by logarithms of Q and ρ, corresponding in Mellin space to inverse powers of M and N, respectively. This may be seen directly by considering Laurent expansions around $M = N = 0$ of the integrands of (2.10) and (2.14): every extra inverse power of M or N must be compensated by a positive power from expansion of the exponential, yielding an extra factor of t or ξ. These logarithms are at most single logarithms, in the sense that in perturbation theory there is at most one extra logarithm of each type whenever there is an extra power of α_s: a typical contribution to the integrand is $\alpha_s^l M^{-m} N^{-n}$ where $m, n \leqslant l$. To obtain meaningful results in perturbation theory these logarithms must be resummed (at LO, where $m+n = 2l$, NLO, where $m+n = 2l+1$, etc.) and factored into the gluon distribution $G(M, N)$. In particular without resummation the GLAP splitting function is unstable in the small x region, while the BFKL kernel is unstable in both the collinear and anti-collinear regions, which means that for reasonable values of α_s it is also unstable in the small x region [6].

Resummation of the transverse and longitudinal logarithms $t = \log Q^2/\Lambda^2$ and $\xi = \log 1/\rho$ proceeds by solution of the GLAP and BFKL equations respectively:

$$\frac{dG}{dt} = \int_\rho^1 \frac{dx}{x} P\left(\frac{\rho}{x}, \alpha_s\left(Q^2\right)\right) G\left(x, Q^2\right), \tag{2.15}$$

where P is the gluon splitting function, and

$$\frac{d\mathcal{G}}{d\xi} = \int_0^\infty \frac{dk^2}{k^2} \mathcal{K}\left(\frac{k^2}{Q^2}, \alpha_s\left(k^2\right)\right) \mathcal{G}\left(x, k^2\right), \tag{2.16}$$

where $\mathcal{K}$ is the (angular averaged) BFKL kernel. Taking double Mellin transforms both equations simplify to algebraic equations, since the convolutions reduce to products and the derivatives to factors of M and N respectively:

$$\begin{aligned} MG(N, M) &= G_0(N) + \gamma(N; \hat{\alpha}_s) G(N, M), \\ NG(N, M) &= \bar{G}_0(M) + M^{-1} \chi(M, \hat{\alpha}_s) MG(N, M), \end{aligned} \tag{2.17}$$

where γ and χ are the Mellin transforms of the respective kernels

$$\gamma(N; \alpha_s) \equiv \int_0^1 \frac{dx}{x} x^N P(x; \alpha_s),$$

$$\chi(M;\hat{\alpha}_s) \equiv \int_0^\infty \frac{dk^2}{k^2}\left(\frac{k^2}{Q^2}\right)^M \mathcal{K}\left(\frac{k^2}{Q^2},\alpha_s\left(k^2\right)\right), \tag{2.18}$$

and $G_0(N)$, $\bar{G}_0(M)$ are (non-perturbative) boundary conditions. The transform of the BFKL equation has been written in terms of the integrated distribution using Eq. (2.8).

The main complication in the derivation of Eqs. (2.17) from Eqs. (2.15), (2.16) is the running of the coupling: in Mellin space $\alpha_s(t)$ becomes an operator

$$\hat{\alpha}_s \equiv \alpha_s\left(-\frac{\partial}{\partial M}\right). \tag{2.19}$$

This leads to various difficulties, discussed at length in Refs. [11,12,21–23]. In the remainder of this section we sidestep this issue, and consider the coupling to be fixed.

At fixed coupling, $\hat{\alpha}_s \to \alpha_s$, and the evolution equations have the simple algebraic solution

$$G(N,M) = \frac{1}{M-\gamma(N;\alpha_s)}G_0(N) = \frac{1}{N-\chi(M;\alpha_s)}\bar{G}_0(M). \tag{2.20}$$

Since the leading twist perturbative singularities can always be factorised from the singularities in the non-perturbative boundary conditions, the poles in the perturbative factors must coincide: at the pole

$$M = \gamma(N;\alpha_s), \quad N = \chi(M;\alpha_s). \tag{2.21}$$

The functions γ and χ must thus satisfy the consistency conditions

$$M = \gamma\big(\chi(M;\alpha_s);\alpha_s\big), \quad N = \chi\big(\gamma(N;\alpha_s);\alpha_s\big), \tag{2.22}$$

i.e. as functions of their main arguments $\gamma = \chi^{-1}$, $\chi = \gamma^{-1}$. These are the duality relations [8,14,24,25]: χ determines the high energy ($N=0$) singularities of γ, just as γ determines the collinear ($M=0$) singularities of χ. For example, if $\gamma \sim \alpha_s/N$, $\chi \sim \alpha_s/M$ and vice versa. Conservation of longitudinal momentum implies that $\gamma(1,\alpha_s) = 0$ to all orders in perturbation theory: duality then tells us that $\chi(0;\alpha_s) = 1$ to all orders in perturbation theory, i.e. that the collinear ($M=0$) singularities in the expansion of $\chi(M;\alpha_s)$ in powers of α_s resum to unity [9].

Using these ideas, and the symmetry under the exchange of Q and k of the BFKL kernel (which in Mellin space translates into a symmetry under $M \to 1-M$ [7]), it is possible to use the known results for the GLAP anomalous dimension $\gamma(N;\alpha_s)$ at LO and NLO in powers of α_s to resum the collinear ($Q^2 \gg k^2$, thus $M=0$) and anti-collinear ($Q^2 \ll k^2$, thus $M=1$) singularities in the BFKL kernel $\chi(M;\alpha_s)$ at LO and NLO. Indeed the resummation of these singularities is essential to obtain a meaningful expansion of the kernel for reasonable values of α_s. The resummed kernel then in turn through duality gives an anomalous dimension in which the high energy $N=0$ singularities are also resummed. This resummed anomalous dimension can then be used to evolve an initial (integrated) gluon distribution at small x [9,26].

The small-x behaviour of the fixed coupling anomalous dimension (or rather its associated splitting function) is given by the behaviour around the minimum of $\chi(M,\alpha_s)$: fixed coupling duality implies that this leads to a square root branch cut at $N = c(\alpha_s) \equiv \chi(\frac{1}{2};\alpha_s)$, at which the anomalous dimension rises to one half:

$$\gamma(N;\alpha_s) \sim \frac{1}{2} - \sqrt{\frac{N-c(\alpha_s)}{\frac{1}{2}\kappa(\alpha_s)}}, \tag{2.23}$$

where $\kappa(\alpha_s) \equiv \chi''(\frac{1}{2}, \alpha_s)$ is the curvature at the minimum. This cut in turn gives rise to the famous $x^{-c(\alpha_s)}$ growth in the splitting function.

Fixed coupling duality may also be used to resum the high energy logarithms in hard cross-sections. Since all the collinear and high energy logarithms have now been absorbed into the integrated gluon distribution, the hard cross-sections are regular in both N and M close to the origin, and may thus be Taylor expanded: for example

$$C(N, M; \alpha_s) = \sum_{l=1}^{\infty} \sum_{m=0}^{\infty} c_m^l(N) \alpha_s^l M^m,$$
$$H(N, M_1, M_2) = \sum_{l=2}^{\infty} \sum_{m_1=0}^{\infty} \sum_{m_2=0}^{\infty} h_{m_1 m_2}^l(N) \alpha_s^l M_1^{m_1} M_2^{m_2}, \tag{2.24}$$

where $c_m^l(N)$ and $h_{m_1 m_2}^l(N) = h_{m_2 m_1}^l(N)$ are also regular in the neighbourhood of $N = 0$. The only singularity close to the origin is thus that in $G(N, M)$, i.e. (2.20), and this may be used to perform one of the photoproduction inverse Mellin transforms (2.10), or two of the hadroproduction inverse Mellin transforms (2.14). The usual procedure is to perform the integrals over M in this way, leaving the single integral over N to be done numerically:

$$\Sigma_{\gamma h}(\rho, Q) = \int_{-i\infty}^{i\infty} \frac{dN}{2\pi i} e^{\xi N} e^{t\gamma(N;\alpha_s)} C\big(N, \gamma(N;\alpha_s); \alpha_s\big) G_0(N),$$
$$\Sigma_{hh}(\rho, Q) = \int_{-i\infty}^{i\infty} \frac{dN}{2\pi i} e^{\xi N} e^{2t\gamma(N;\alpha_s)} H\big(N, \gamma(N;\alpha_s), \gamma(N;\alpha_s); \alpha_s\big) G_0(N)^2. \tag{2.25}$$

Note that since $\gamma(N;\alpha_s)$ contains resummed poles in N (i.e. terms of the form $\alpha_s^l N^{-n}$, with $n \leqslant l$) this procedure effectively resums the high energy singularities in the collinearly factorised hard cross-sections, obtained by expanding $C(N, \gamma(N;\alpha_s); \alpha_s)$ and in $H(N, \gamma(N;\alpha_s), \gamma(N;\alpha_s); \alpha_s)$ respectively in powers of α_s [2,15,25]. Conversely, comparing Eqs. (2.25) with the more conventional expressions

$$\Sigma_{\gamma h}(\rho, Q) = \int_{-i\infty}^{i\infty} \frac{dN}{2\pi i} e^{\xi N} e^{t\gamma(N;\alpha_s)} c(N;\alpha_s) G_0(N),$$
$$\Sigma_{hh}(\rho, Q) = \int_{-i\infty}^{i\infty} \frac{dN}{2\pi i} e^{\xi N} e^{2t\gamma(N;\alpha_s)} f(N;\alpha_s) G_0(N)^2, \tag{2.26}$$

obtained in collinear factorization, we see that

$$c(N;\alpha_s) = \sum_{l=0}^{\infty} \alpha_s^l c_l(N) = C\big(N, \gamma(N;\alpha_s); \alpha_s\big),$$
$$f(N;\alpha_s) = \sum_{l=0}^{\infty} \alpha_s^l f_l(N) = H\big(N, \gamma(N;\alpha_s), \gamma(N;\alpha_s); \alpha_s\big). \tag{2.27}$$

Thus by substituting the fixed order expansion $\gamma(N;\alpha_s) = \sum_{l=0}^{\infty} \alpha_s^l \gamma_l(N)$ into the expansions (2.24) of the right-hand side of (2.27) the high energy singularities of the fixed order hard cross-sections $c_l(N)$ and $f_l(N)$ may be economically computed. This makes matching to the fixed order calculations particularly straightforward.

This is the procedure used in most previous studies [2,15–17,25,26] of the effects of high energy resummation on high energy cross-sections. It leads to a strong growth in cross-sections, particularly hadronic cross-sections, due to infrared singularities at positive values of M which, unlike the collinear singularities near $M = 0$, have not been resummed into the perturbative evolution. It is the nature of these infrared singularities, and the correct treatment of them, that is the main subject of this paper. First however we must consider how this simple picture is modified when the coupling runs.

2.5. Duality at running coupling

When the coupling runs the evolution equations (2.17) become differential equations in M, since the running coupling transforms to a differential operator (2.19). This operator commutes with N but not with M:

$$[\hat{\alpha}_s, M] = \beta(\hat{\alpha}_s), \tag{2.28}$$

where $\beta(\alpha_s) = -\alpha_s^2\beta_0 + \cdots$ is the QCD beta-function. This means that the BFKL operator $\chi(M;\hat{\alpha}_s)$ must be defined very carefully: different orderings of $\hat{\alpha}_s$ and M will give different results, because the arguments of the couplings will be different [22].

It was show some time ago both by saddle point arguments for the Mellin inversion [27] and by explicit solution of the M-space differential equation [28] that when the coupling runs, the naive duality (2.22) is modified by terms proportional to β: for example at NLLx, writing $\chi(M,\alpha_s) = \alpha_s\chi_0(M) + \alpha_s^2\chi_1(M) + \cdots$,

$$\chi_1 \to \chi_1 + \beta_0 \frac{\chi_0''\chi_0}{2\chi_0'}, \tag{2.29}$$

where the primes denote derivatives with respect to M. In Ref. [22] it was shown that the fixed coupling duality (2.22) may be extended formally to relations between the operators $\gamma(N;\hat{\alpha}_s)$ and $\chi(M;\hat{\alpha}_s)$, which may then be used to generate systematically running coupling corrections using a purely algebraic algorithm, order by order in perturbation theory. This technique was used recently [23] to compute an estimate of the leading twist BFKL kernel χ_2 at NNLLx.

When the coupling runs it becomes important to specify carefully the factorization scheme, since a redefinition of the gluon distribution $G(N,M) \to Z(M)G(N,M)$ changes $\chi(M,\hat{\alpha}_s)$ by a commutator:

$$\chi(M,\hat{\alpha}_s) \to \chi(M,\hat{\alpha}_s) + Z^{-1}(M)\big[\chi(M;\hat{\alpha}_s), Z(M)\big]. \tag{2.30}$$

It is thus possible to shuffle the running coupling terms between the evolution and the hard cross-section. In this paper we will use the $\mathrm{Q_0\overline{MS}}$ scheme [29–31], a variant on the $\overline{\mathrm{MS}}$ scheme in which all the running coupling terms are absorbed into the evolution. The two schemes are equivalent in fixed order perturbation theory at LO, NLO and NNLO, but begin to differ at NNNLO.

Note that provided $Z(M)$ is regular at $M = 0$ the second term on the right-hand side of (2.30) is subleading compared to the first, since the commutator necessarily introduces an extra power

of $\hat{\alpha}_s$ (see (2.28), and note that $\beta(\alpha_s) = -\beta_0\alpha_s^2 + O(\alpha_s^3)$). This means that if we work at NLLx in the resummation of the singularities, it is only necessary to consider the hard cross-sections $C(N, M; \hat{\alpha}_s)$ and $H(N, M_1, M_2; \hat{\alpha}_s)$ at LLx: terms at NLLx in the cross-section are NNLLx in the evolution [2,28]. Similarly to this order we may ignore the running of α_s in the hard cross-section, setting $\hat{\alpha}_s \to \alpha_s$ up to subleading terms.

Away from the region of very small x the running coupling corrections to naive duality are small. However in the small x limit, they become very large. This may be seen immediately from (2.29): at small x and fixed coupling, the integrals over M are dominated by the minimum of $\chi(M, \alpha_s)$, and thus by $M \sim 1/2$, i.e. the region in which $\chi_0'(M) \sim 0$ and the correction (2.29) becomes large. It was thought at one time that these terms become so large that they drive instabilities in the gluon distribution leading to negative cross-sections [10,30,32,33]. However these instabilities are due to diffusion into the infrared: if the singularities are resummed, they may be factorised into the (non-perturbative) initial distribution, resulting in stable evolution [11–13].

This further resummation of the running coupling singularities at $M = 1/2$ is accomplished by expanding around the minimum of χ, solving for $G(N, M)$ and then performing the inverse Mellin with respect to M exactly, rather than using a saddle point expansion. The simplest version of this argument gives rise to an Airy function [21]: a full calculation [12] summing up the leading singularities in β_0 gives the running coupling resummed anomalous dimension

$$\gamma_B(N; \alpha_s) = \frac{1}{2} - \beta_0\bar{\alpha}_s + \frac{1}{A}\frac{K_{2B}'((\beta_0\alpha_s A)^{-1})}{K_{2B}((\beta_0\alpha_s A)^{-1})}, \tag{2.31}$$

where A and B are simple functions of α_s and N computed from the value of $\chi(M, \alpha_s)$ and its curvature at the minimum, and $K_\nu(z)$ is the Bateman function. The small x behaviour resulting from (2.31) is qualitatively different from that obtained with the fixed coupling result (2.23), since the cut is replaced by a simple pole located at $N = c_B(\alpha_s)$, with $c_B(\alpha_s)$ given by the rightmost zero of the Bateman function. Since $c_B(\alpha_s)$ is rather less than $c(\alpha_s)$, the $x^{-c(\alpha_s)}$ growth of the splitting function at small x is softened by the running coupling effects to $x^{-c_B(\alpha_s)}$ [12]. However since the new singularity is now a pole and not a cut M can now grow indefinitely rather than saturating at $M = 1/2$: in effect the region between $M = 0$ and $M = 1/2$ is stretched to infinity so that the effective $\chi(M; \alpha_s)$ (the naive dual of $\gamma(N; \alpha_s)$) is analytic for all $M > 0$.

By combining the running coupling resummation with a collinear and anti-collinear resummation of $\chi(M; \alpha_s)$ using running duality, a completely resummed anomalous dimension may be computed, and used to resum both high energy and collinear singularities in the gluon distribution at LO and NLO [12,13]. Such a NLO resummed gluon distribution is plotted in Fig. 4 for x down to 10^{-10} and Q up to 50 TeV. The initial distribution was chosen to be proportional to $x^{-0.18}(1-x)^5$ at 2 GeV, with the first moment (i.e. the integrated longitudinal momentum) normalised to unity. We take $\alpha_s(m_Z) = 0.118$, $\alpha_s(Q)$ evaluated using standard two loop running with thresholds at m_b and m_t. For comparison we also plot the same distribution evolved using the LO and NLO GLAP anomalous dimensions. All evolution is performed with n_f set to zero in the anomalous dimensions, consistent with our suppression of all quark induced processes. It can be seen from the plot that the effect of the resummation is modest, even over such a wide kinematic range, and is generally such as to smoothly soften the growth at small x and large Q^2.

2.6. Soft singularities in hard cross-sections

All that remains to be done is to combine this resummed gluon distribution with a hard cross-section. However when the coupling runs it is no longer so easy to justify the use of the pole

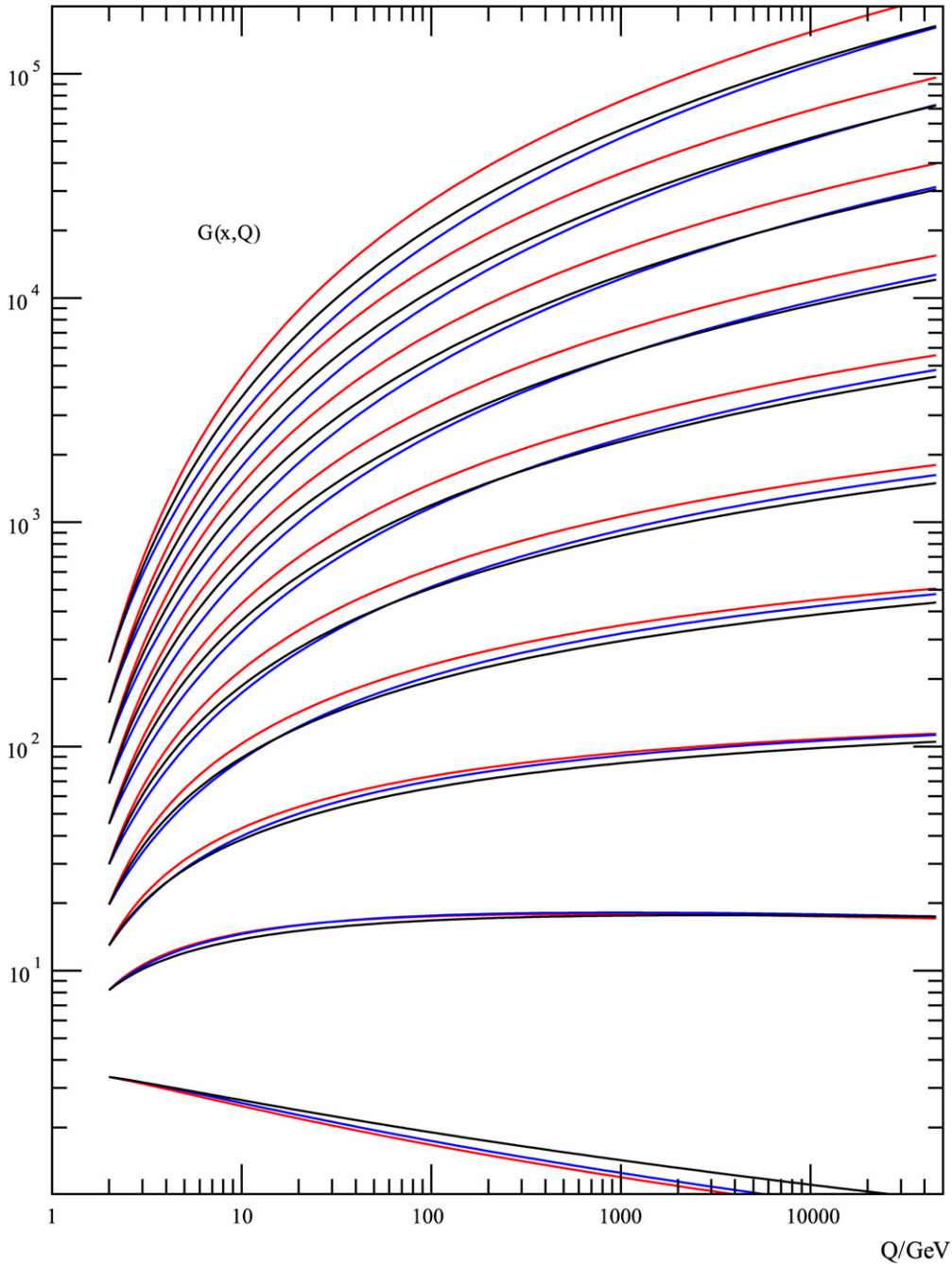

Fig. 4. The gluon distribution $G(x, Q)$ plotted against Q in GeV for $x = 10^{-10}, 10^{-9}, \ldots, 0.01, 0.1$ (from top to bottom). The blue curves are evolved with the NLO resummation described in the text: the black and red curves are with LO and NLO GLAP evolution respectively. (For interpretation of the references to colour in this figure legend, the reader is referred to the web version of this article.)

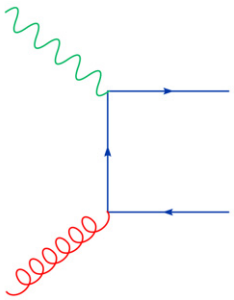

Fig. 5. Photoproduction of heavy quarks. The photon is on-shell, while the gluon is off-shell by an amount k^2, in order to calculate the impact factor $C(N, M)$. In electroproduction the photon would also be taken off-shell.

approximation (2.20) to perform the integrals over M in (2.10) and (2.14) as we did at fixed coupling, Eq. (2.26), since for the gluon distribution itself we know that at small x the pole approximation no longer gives the correct asymptotic behaviour. Moreover, since when the coupling runs the resummed anomalous dimension $\gamma(N, \alpha_s)$ rises indefinitely as N decreases, the position $M = \gamma(N, \alpha_s)$ of the pole in the evolved gluon will also grow large, and thus eventually the contour (which is always to the right of this pole) will become entangled with the various infrared singularities in the hard cross-sections.

Consider first the photoproduction or electroproduction hard cross-section $C(N, M)$, which may be computed at leading order from the graph shown in Fig. 5. The hard scale Q is then the mass of the quark (for photoproduction of heavy quarks), or the photon virtuality (for electroproduction). The incoming gluon has virtuality k^2. At very high energies $S \gg Q^2$, relevant values of N should be small, so can in the first instance be neglected. Then considered as a function of M, $C(0, M)$ is regular near $M = 0$ (since the collinear singularities, with $Q^2 \gg k^2$, have already been absorbed in the gluon distribution), but has poles at $M = -1, -2, \ldots$ and $M = 1, 2, 3, \ldots$. The poles at negative values of M correspond to higher twist singularities: they lead to power corrections in inverse powers of Q^2, which are not relevant here. The poles at positive values of M correspond instead to process dependent infrared (anti-collinear) singularities with $Q^2 \ll k^2$. It is these singularities that enhance the cross-section at high energy.

When the coupling is fixed, the anomalous dimension for the gluon evolution saturates at the cut, and thus at high energy the dominant contribution to the M integral is from the region $M = 1/2$. The resummation K-factor may be then be estimated at high energy to be $\frac{C(0,1/2)}{C(0,0)} = \frac{27\pi^2}{56} \sim 4.8$, a significant enhancement [15]. However when the coupling runs, there is no such saturation, and the pole approximation to the integration over M breaks down at high energy, since the pole at $M = \gamma(N, \alpha_s)$ in the evolved gluon can then approach the pole at $M = 1$ in the hard cross-section, and the contour gets pinched between them. We must then attempt to perform the integration exactly, and afterwards factor out the gluon distribution: resummation of the hard cross-section is thus rather more difficult than it was at fixed coupling.

This difficulty becomes much worse when we consider hadroproduction. Once again we focus on the singularities of the impact factor $H(0, M_1, M_2)$ in the double-Mellin plane of M_1 and M_2. This may be obtained from the graphs in Fig. 6 (hadroproduction of heavy quarks, so Q is the quark mass), or Figs. 6 and 7 (inclusive jets, so Q is the transverse momentum of the jets). Again the region around the origin is regular, and there are higher twist poles at $M_1, M_2 = -1, -2, \ldots$ and infrared singularities at $M_1, M_2 = 1, 2, \ldots$. However now we also have lines of infrared

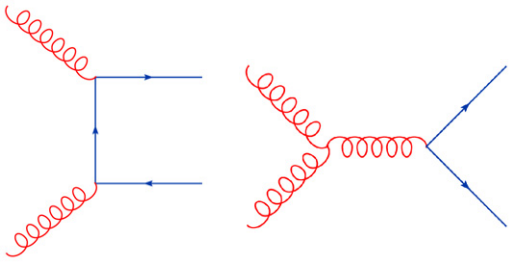

(a) (b)

Fig. 6. Hadroproduction of heavy quarks: (a) the "Abelian" diagram, with initial state radiation and (b) the "non-Abelian" diagram with final state radiation. Both incoming gluons are taken off-shell by amounts k_1^2 and k_2^2 in order to calculate the impact factor $H(0, M_1, M_2)$. The same graphs give hadroproduction of quark jets.

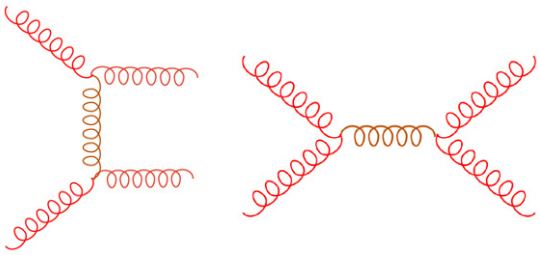

(a) (b)

Fig. 7. Hadroproduction of gluonic jets: (a) the "Abelian" diagram with initial state radiation and (b) the "non-Abelian" diagram with final state radiation. Both incoming gluons are taken off-shell. The two final state gluons are on-shell, with a specified p_T. The four gluon vertex diagram is not shown, since it is nonsingular.

singularities at $M_1 + M_2 = 1, 2, \ldots$: for example the heavy quark hadroproduction impact factor

$$H(M_1, M_2) \sim \alpha_s^2 \frac{\pi}{16} \frac{1}{(1 - M_1 - M_2)^3}, \tag{2.32}$$

when $M_1 + M_2 \sim 1$ [15,16,27]. It is easy to see why this occurs by noting the form of the Mellin transform Eq. (2.12): an infrared singularity when $Q^2 \ll k_1^2, k_2^2$ will become a singularity at $M_1 + M_2 = 1, 2, \ldots$.

The degree of this singularity will depend on the nature of the infrared singularities of the individual graphs making up the process. The graphs with initial state radiation, Figs. 6(a) and 7(a), both have a single (anti)collinear singularity similar to that in photoproduction Fig. 5. However the singularity structure of the non-Abelian graphs with final state radiation Figs. 6(b) and 7(b) is more complicated. Firstly there is a soft singularity when the internal (timelike) gluon goes on-shell: the denominator of the propagator is $s = x_1 x_2 S - (\mathbf{k}_1 + \mathbf{k}_2)^2$, and the singularity arises when $x_1 x_2 S \simeq (\mathbf{k}_1 + \mathbf{k}_2)^2 \ll \mathbf{k}_1^2 \simeq \mathbf{k}_2^2$ [15]. On top of this there is the usual collinear (heavy quark production) or soft (jet production) singularity for the emission of the final state partons, so altogether we find the triple pole Eq. (2.32). Note that this kind of singularity is thus generic to most gluon–gluon hard cross-sections. In fact it is the dominant singularity, providing most of the cross-section at very high energy.

To evaluate the cross-section, we must perform the double Mellin inversion Eq. (2.14). When the coupling is fixed, M_1 and M_2 both try to saturate at $M_1 = M_2 = \frac{1}{2}$, and thus touch the

singularity. This produces a strong enhancement of the cross-section [15], stronger even than the BFKL growth. If M_1 and M_2 can grow beyond one half, as one expects at running coupling, the contours are pinched, and the cross-section seems to grow as fast as $\rho^{-2\alpha_s}$ [16]. However this dramatic growth is also very unstable, in particular to N dependent corrections, since these split the triple pole into a separate double pole (at $M_1 + M_2 = 1 + N$) and a single pole (at $M_1 + M_2 = 1$). This instability is a sure sign that the resummation is not under control. Indeed, when the coupling runs, the whole line of singularity become accessible (since both M_1 and M_2 may become large), and furthermore becomes entangled with the collinear regions (since at $M_1 \sim 0$, $M_2 \sim 1$ and vice versa).

So somehow we need a more reliable way of computing the integrals over M_1 and M_2. Since the singularity (2.32) does not factorise into a function of M_1 times a function of M_2, we actually need to perform both integrals simultaneously, and then factorise out the gluon distributions afterwards to obtain the resummation of the hard cross-section.

In the rest of this paper we will show how a simple trick may be used to solve this problem, first for photoproduction and electroproduction (Section 3) and then for hadroproduction (Section 4). We consider processes with a single incoming gluon first because they are simpler: the more important hadroproduction processes will then be dealt with by a straightforward extension of essentially the same idea.

3. Photoproduction and electroproduction

3.1. Evaluating the cross-section

Consider first a photoproduction or electroproduction cross-section at high energy, and thus small ρ, but still far from the high energy limit. Then we might expect M to remain "small" in some sense, and consider approximating the hard cross-section $C(N, M; \alpha_s)$ by the first few terms in its Taylor expansion (2.24). The cross-section (2.10) may then be written

$$\Sigma_{\gamma\mathrm{h}}(\rho, Q) = \int_{-i\infty}^{i\infty} \frac{dN}{2\pi i} e^{\xi N} \Sigma_{\gamma\mathrm{h}}(N, t), \tag{3.1}$$

where

$$\Sigma_{\gamma\mathrm{h}}(N, t) = \alpha_s(t) \sum_{m=0}^{\infty} c_m^1(N) \int_{-i\infty}^{i\infty} \frac{dM}{2\pi i} e^{tM} M^m G(N, M), \tag{3.2}$$

where we have kept only the leading term in the expansion in α_s, and (optimistically) changed the order of integration and summation over m, in order to do the integrals term by term. However for the first term this is an integral we already know:

$$G(N, t) = \int_{-i\infty}^{i\infty} \frac{dM}{2\pi i} e^{tM} G(N, M), \tag{3.3}$$

and consequently for all $m = 0, 1, 2, \ldots$

$$\int_{-i\infty}^{i\infty} \frac{dM}{2\pi i} e^{tM} M^m G(N, M) = \frac{\partial^m}{\partial t^m} G(N, t). \tag{3.4}$$

However the general solution of the evolution equation (2.15) is simply

$$G(N,t) = \exp\left(\int_0^t dt'\,\gamma\big(N,\alpha_s(t')\big)\right) G_0(N), \tag{3.5}$$

so all the partial derivatives in (3.4) may be evaluated in terms of the anomalous dimension and its derivatives:

$$\begin{aligned}
&\frac{\partial}{\partial t} G(N,t) = \gamma(N,t) G(N,t),\\
&\frac{\partial^2}{\partial t^2} G(N,t) = \big(\gamma^2 + \dot\gamma\big) G(N,t),\\
&\frac{\partial^3}{\partial t^3} G(N,t) = \big(\gamma^3 + 3\gamma\dot\gamma + \ddot\gamma\big) G(N,t), \ldots,
\end{aligned} \tag{3.6}$$

where the dot denotes partial derivatives with respect to t.

Note that $\dot\gamma$ is formally subleading compared to γ, since

$$\frac{\partial}{\partial t} = \beta(\alpha_s)\frac{\partial}{\partial \alpha_s} = -\beta_0 \alpha_s^2 \frac{\partial}{\partial \alpha_s}, \tag{3.7}$$

so every time we differentiate with respect to t we add a power of α_s. So up to subleading terms partial derivatives of $G(N,t)$ with respect to t simply result in powers of $\gamma(N;\alpha_s(t))$, and combining Eq. (3.2) with (3.4) we find

$$\Sigma_{\gamma\mathrm{h}}(N,t) = \alpha_s(t) \sum_{m=0}^{\infty} c_m^1(N) \frac{\partial^m}{\partial t^m} G(N,t) = \alpha_s(t) C\big(N, \gamma\big(N,\alpha_s(t)\big)\big) G(N,t). \tag{3.8}$$

So provided we are not close to a pole, we find the same result when the coupling runs as we found at fixed coupling case through the pole dominance argument (2.26).

Formally this method works provided the series (3.8) converges. To see whether this is likely in practice, we plot in Fig. 8 the first and second derivatives of the gluon distributions Fig. 4, normalised to G: indeed the derivatives are much less than one for all but the lowest values of x and Q. Moreover the second derivatives are much smaller than the first, suggesting that the series converges rather rapidly. In addition derivatives for the NLO resummed gluons are rather smaller at low x and Q than those for the NLO GLAP gluons, essentially because they evolve rather more slowly. It follows that at all but the smallest x and Q we may use Taylor expansions in M, and we will show repeated examples of this in what follows. It is worth noting in parenthesis that Taylor expansion in M is little different at high energy to the usual fixed order expansion of the hard cross-section (2.27), since it is only through the M dependence of $C(N,M;\alpha_s)$ that small N singularities can be introduced, and at high energy it is these that dominate the cross-section.

3.2. Resumming an infrared singularity

Now consider what happens when $C(N,M;\alpha_s)$ has a pole near $M=1$, so that the Taylor expansion around $M=0$ has radius of convergence one. This will generally be the case: such a singularity corresponds to logarithms of k^2/Q^2 as $k^2 \to 0$. We will then need to do integrals of

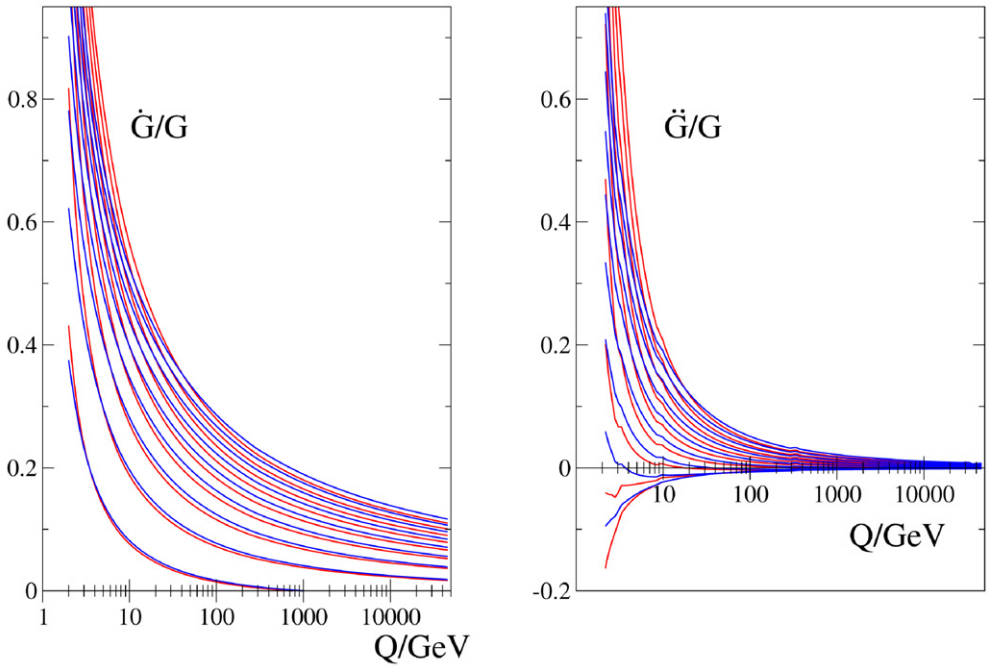

Fig. 8. The first (left) and second (right) derivatives with respect to t of the gluon distributions $G(x, Q)$ plotted in Fig. 4, normalised to G, plotted against Q in GeV, for $x = 10^{-10}, 10^{-9}, \ldots, 0.01$ (from top to bottom). Again the blue curves are with NLO resummed evolution, the red with NLO GLAP evolution. (For interpretation of the references to colour in this figure legend, the reader is referred to the web version of this article.)

the form

$$\Sigma^n_{\gamma\mathrm{h}}(N,t) = \int_{-i\infty}^{i\infty} \frac{dM}{2\pi i} \frac{1}{(1-M)^n} e^{tM} G(N,M), \tag{3.9}$$

for $n = 1, 2, \ldots$. We can perform these integrals exactly using a simple trick [34]: we write

$$\frac{1}{(1-M)^n} = \frac{1}{n!} \int_0^\infty d\tau\, \tau^{n-1} e^{-\tau(1-M)}, \tag{3.10}$$

thereby exponentiating the dependence on M and transferring possible singularities in the complex variable M to singularities in the integration over the real variable τ. Substituting (3.10) into (3.9) the M integration is now indeed trivial:

$$\begin{aligned}\Sigma^n_{\gamma\mathrm{h}}(N,t) &= \int_{-i\infty}^{i\infty} \frac{dM}{2\pi i} \frac{1}{n!} \int_0^\infty d\tau\, \tau^{n-1} e^{-\tau + M(t+\tau)} G(N,M) \\ &= \frac{1}{n!} \int_0^\infty d\tau\, \tau^{n-1} e^{-\tau} G(N, t+\tau),\end{aligned} \tag{3.11}$$

where in the second line we exchanged the order of the integrations over M and τ and performed the integration over M. Since when the coupling runs the growth of $G(N,t)$ with t is rather gentle (no greater than a power of t), the τ integral converges for all t. At small x the $M=1$ singularity thus always leads to a modest enhancement of $G(x,t)$, since the growth with t is monotonic.

We may factorise this result using Eq. (3.5): this gives

$$\Sigma^n_{\gamma\mathrm{h}}(N,t)=\left[\frac{1}{n!}\int_0^\infty d\tau\,\tau^{n-1}\exp\left(-\tau+\int_0^\tau dt'\,\gamma\big(N,\alpha_s(t+t')\big)\right)\right]G(N,t). \tag{3.12}$$

The expression in square brackets is thus the resummed hard cross-section $C(N;\alpha_s(t))$.

Note that if we Taylor expand $G(N,t+\tau)$ in (3.11) in powers of τ

$$\begin{aligned}\frac{1}{n!}\int_0^\infty d\tau\,\tau^{n-1}e^{-\tau}G(N,t+\tau)&=\int_0^\infty d\tau\sum_{m=0}^\infty\frac{\tau^{m+n-1}}{n!m!}e^{-\tau}\frac{\partial^m}{\partial t^m}G(N,t)\\&=\sum_{m=0}^\infty\frac{(m+n)!}{n!m!}\frac{\partial^m}{\partial t^m}G(N,t),\end{aligned} \tag{3.13}$$

where in the second line we exchanged the order of summation and integration in order to perform the integrals over τ. The result is of course precisely what one gets by first Taylor expanding $1/(1-M)^n$ in Eq. (3.9) about $M=0$ and then using Eq. (3.4). However the resulting series is useful only if $\gamma(N,t)$ and its derivatives are sufficiently small, as discussed in the previous section, whereas the integral representation Eq. (3.11) always converges. When the series diverges, the integral representation resums it.

It is instructive to consider explicitly two analytic examples of how this works in practice. First consider what happens at fixed coupling: then at leading order $G(N,t)=e^{\gamma(N;\alpha_s)t}G_0(N)$, so taking $n=1$ for simplicity

$$\Sigma^1_{\gamma g}(N,t)=\int_0^\infty d\tau\,e^{-\tau}e^{\gamma(N;\alpha_s)(t+\tau)}G_0(N)=\frac{1}{1-\gamma(N,\alpha_s)}G(N,t). \tag{3.14}$$

This is precisely the result expected from the pole dominance argument described in Section 2.4: M in the hard cross-section is replaced by $\gamma(N;\alpha_s)$ according to Eq. (2.21). So the pole at $M=1$ results in a new pole when $\gamma(N;\alpha_s)=1$, to the right of the rightmost pole in $\gamma(N;\alpha_s)$: for example if $\gamma(N;\alpha_s)=\alpha_s/N$, the new pole is at $N=\alpha_s$. Thus on performing the N integration (3.1) the cross-section $\Sigma(\rho,Q)$ will exhibit a powerlike enhancement at high energy, growing faster than $G(\rho,Q)$.

Now consider what happens instead when the coupling runs: if we take for example $\gamma(N;\alpha_s(t))=\alpha_s(t)\gamma_0(N)$, and $\alpha_s(t)=1/\beta_0 t$, then $G(N,t)=t^{\gamma_0(N)/\beta_0}G_0(N)$, and

$$\begin{aligned}\Sigma^1_{\gamma\mathrm{h}}(N,t)&=\int_0^\infty d\tau\,e^{-\tau}(t+\tau)^{\gamma_0(N)/\beta_0}G_0(N)\\&=t^{-\gamma_0(N)/\beta_0}e^t\Gamma\big(1+\beta_0^{-1}\gamma_0(N),t\big)G(N,t),\end{aligned} \tag{3.17}$$

where $\Gamma(a,t)\equiv\int_t^\infty ds\,s^{a-1}e^{-s}$ is the incomplete gamma function. The only finite singularity in $\Gamma(a,t)$ is a branch cut from $t=0$ down the negative real axis: for t real and positive, $\Gamma(a,t)$

is entire in a. Consequently the only singularities of $\Sigma^1_{\gamma\mathrm{h}}(N,t)$ are those of $\gamma_0(N)$: in particular there is no new singularity when $\gamma(t)=\alpha_s(t)\gamma_0(N)\sim 1$. So when the coupling runs, $\Sigma(\rho,Q)$ rises asymptotically in the same way as $G(\rho,Q)$.

It is easy to see that this smoothing away of the $M=1$ pole (and indeed of any pole at $M=m_0$, provided only that m_0 is real and positive) is a generic feature when the coupling runs: the key ingredient is that $G(N,t)$ is a regular function of $\ln t$ rather than of t. As recalled in Section 2.5 the interval $M\in(0,1/2)$ is then stretched to $(0,\infty)$, and so singularities at $M=1,2,\ldots$ are effectively pushed out to infinity. This means that when the coupling runs the expansion of the hard cross-section around $M=0$ provides a good approximation to the exact result after only a few terms: the running coupling resummation of the $M=1/2$ singularity Eq. (2.29) in the evolution effectively deals with all the singularities for $M>1/2$, not only in the evolution but also in the hard cross-section, ensuring that all such singularities are factorised into the initial distribution.

In fact we can show that when the coupling runs, the expansion (3.13) is indeed asymptotic: returning to the specific example (3.15), and using the asymptotic series

$$\Gamma(a,t)\sim t^{a-1}e^{-t}\bigl[1+(a-1)t^{-1}+(a-1)(a-2)t^{-2}+\cdots\bigr], \tag{3.18}$$

as $t\to\infty$, then as $\alpha_s(t)\to 0$

$$\begin{aligned}\Sigma^1_{\gamma\mathrm{h}}(N,t)\sim\Biggl[&1+\gamma(t)+\gamma(t)^2\left(1-\frac{\beta_0}{\gamma_0}\right)\\&+\gamma(t)^3\left(1-\frac{\beta_0}{\gamma_0}\right)\left(1-2\frac{\beta_0}{\gamma_0}\right)+\cdots\Biggr]G(N,t),\end{aligned} \tag{3.19}$$

which is the same series term by term as (3.13) provided we evaluate the derivatives using Eqs. (3.6). So in the running coupling case the expansion in powers of derivatives is indeed an asymptotic series.

To see how well this asymptotic series works in practice, rather than in these simple examples, we define the K-factor as the ratio[1]

$$K_1(\rho)=\frac{\Sigma^1_{\gamma\mathrm{h}}(\rho,Q)}{\Sigma^0_{\gamma\mathrm{h}}(\rho,Q)}, \tag{3.20}$$

where $\Sigma^0_{\gamma\mathrm{h}}(\rho,Q)$ is simply the gluon distribution $G(\xi,t)$. With this definition the dependence on the gluon distribution largely cancels, so one sees the effect of the hard cross-section. Then

$$K_1(\rho)=\frac{1}{G(\xi,t)}\int_{-i\infty}^{i\infty}\frac{dN}{2\pi i}e^{N\xi}\int_0^\infty d\tau\,e^{-\tau}G(N,t+\tau) \tag{3.15}$$

$$=1+\frac{1}{G(\xi,t)}\frac{\partial}{\partial t}G(\xi,t)+\frac{1}{G(\xi,t)}\frac{\partial^2}{\partial t^2}G(\xi,t)+\frac{1}{G(\xi,t)}\frac{\partial^3}{\partial t^3}G(\xi,t)+\cdots, \tag{3.16}$$

where in the first line we used (3.11), and in the second (3.13). Using the resummed gluon distribution shown in Fig. 4 and its derivatives Fig. 8, it is now a simple matter to compute the K-factor, using either (3.15) or the series (3.16). The result is shown in Fig. 9. It can be seen from

[1] Note that this K-factor is not the same as those used in phenomenological applications, which also include a factor due to the difference between LO and higher order partons.

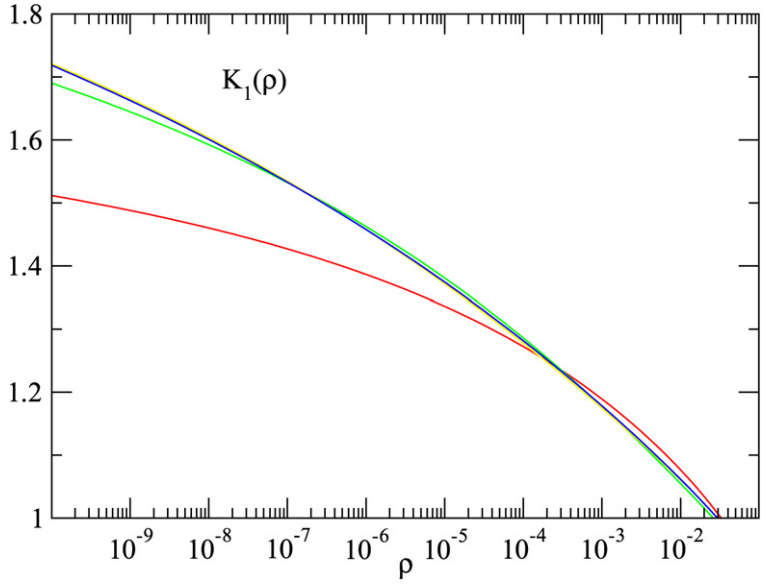

Fig. 9. A generic photoproduction K-factor for a simple pole $1/(1-M)$. The blue (upper) line corresponds to the exact expression Eq. (3.15), while the red, green and yellow lines (from bottom to top) are the NLO, NNLO and NNNLO approximation to it computed by including the second, third and fourth terms respectively of the series (3.16). The hard scale is set at 10 GeV. (For interpretation of the references to colour in this figure legend, the reader is referred to the web version of this article.)

the plot that even a simple pole at $M=1$ gives rise to a quite substantial K-factor, and moreover that the NLO approximation to this K-factor, consisting of only the second term of (3.16), is adequate only for $\rho \gtrsim 10^{-4}$. However the convergence thereafter is very rapid: the NNLO approximation (the first three terms of (3.16)) is very good down to $\rho \sim 10^{-8}$, and the NNNLO approximation (four terms) is difficult to distinguish from the exact result. Thus although the series is only asymptotic, in practice the first few terms give an excellent approximation to the full result.

3.3. *Photoproduction of heavy quarks*

We now consider the inclusive cross-section for the photoproduction of a heavy quark pair. The hard scale in this case is the mass of the heavy quarks: $Q=2m_q$. The off-shell hard cross-section may be calculated from the diagram in Fig. 5: the result in $\mathrm{Q_0\overline{MS}}$ scheme is [35][2]

$$C(N,M) = e_Q^2 \alpha\alpha_s \pi 4^N \frac{14+20N+9N^2+N^3-M(10+7N+N^2)}{3-2M+2N} \times \frac{\Gamma(1-M+N)^3\Gamma(1+M)}{\Gamma(2-2M+2N)\Gamma(4+N)}. \tag{3.21}$$

[2] In Refs. [15,16,35] this function is denoted by $j_\omega(\gamma)$.

When $M=0$ this reduces to the usual $\overline{\rm MS}$ photoproduction cross-section relevant at large ρ, with poles at $N=-1,-\frac{3}{2},-2,\ldots$, while at $N=0$ it reduces to the impact factor [15]

$$C(0,M)=e_Q^2\alpha\alpha_s\frac{\pi}{3}\frac{7-5M}{3-2M}\frac{\Gamma(1-M)^3\Gamma(1+M)}{\Gamma(2-2M)}, \tag{3.22}$$

relevant for calculations at small ρ, i.e. at high energies $S\gg Q^2$, with higher twist poles at $M=-1,-2,\ldots$ and infrared poles at $M=1,\frac{3}{2},2,\ldots$. It is the latter that are relevant for the high energy limit: in particular near $M=1$ we have a double and a simple pole:

$$C(0,M)\sim e_Q^2\alpha\alpha_s\frac{2\pi}{3}\left[\frac{2}{(1-M)^2}-\frac{1}{1-M}+O(1)\right]. \tag{3.23}$$

Expanding Eq. (3.22) about $M=0$ gives the Taylor expansion

$$\begin{aligned}C(0,M)&=e_Q^2\alpha\alpha_s\frac{7\pi}{9}\left(1+\frac{41}{21}M+\frac{244}{63}M^2+\left(\frac{1460}{189}-2\zeta_3\right)M^3+O\big(M^4\big)\right)\\&\simeq e_Q^2\alpha\alpha_s 2.444\big(1+1.952M+3.87M^2+5.32M^3+\cdots\big).\end{aligned} \tag{3.24}$$

This series has quite large coefficients, all of one sign, and growing: one thus expects it to converge rather slowly even for $|M|<1$. This is largely due to the double pole at $M=1$: removing this by hand we find a series with rather smaller coefficients

$$\begin{aligned}C(0,M)&\simeq e_Q^2\alpha\alpha_s\frac{7\pi}{9}\left(\frac{12}{7}\frac{1}{(1-M)^2}-\frac{5}{7}-\frac{31}{21}M-\frac{80}{63}M^2\right.\\&\qquad\left.+\left(\frac{161}{189}-2\zeta_3\right)M^3+O\big(M^4\big)\right)\\&\simeq e_Q^2\alpha\alpha_s 2.444\left(\frac{1.714}{(1-M)^2}-0.714-1.476M-1.27M^2-1.54M^3+\cdots\right).\end{aligned} \tag{3.25}$$

An even better series may be obtained by removing both the double and single poles by hand:

$$\begin{aligned}C(0,M)&\simeq e_Q^2\alpha\alpha_s\frac{7\pi}{9}\left(\frac{12}{7}\frac{1}{(1-M)^2}-\frac{6}{7}\frac{1}{(1-M)}+\frac{1}{7}-\frac{13}{21}M-\frac{26}{63}M^2\right.\\&\qquad\left.+\left(\frac{326}{189}-2\zeta_3\right)M^3+O\big(M^4\big)\right)\\&\simeq e_Q^2\alpha\alpha_s 2.444\left(\frac{1.714}{(1-M)^2}-\frac{0.857}{1-M}+0.143-0.619M-0.41M^2\right.\\&\qquad\left.-0.68M^3+\cdots\right).\end{aligned} \tag{3.26}$$

We can now use these expressions to compute the K-factor for inclusive B photoproduction,

$$K_B(\rho)=\frac{\Sigma^B_{\gamma\rm h}(\rho,m_B)}{\Sigma^O_{\gamma\rm h}(\rho,m_B)}, \tag{3.27}$$

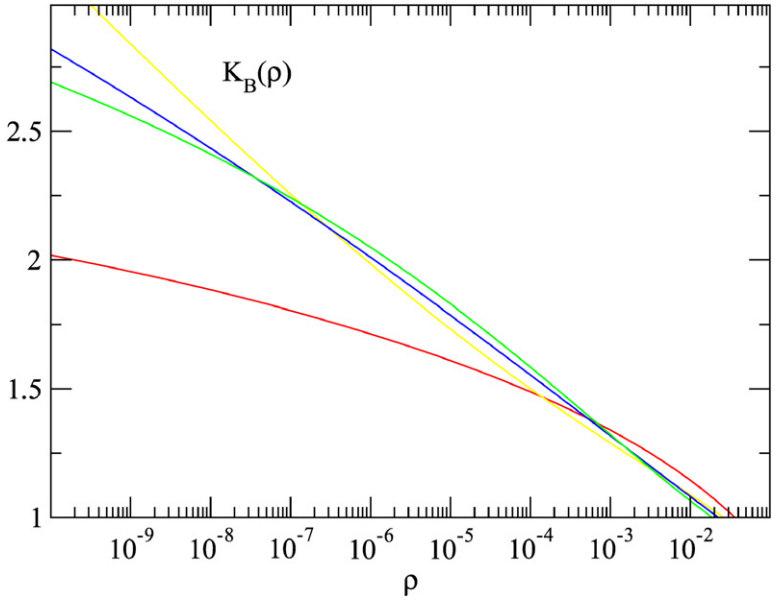

Fig. 10. The K-factor for photoproduction of b quarks. The blue curve (upper) is the resummed result, while the red, green and yellow curves (bottom to top) are the NLO, NNLO and NNNLO fixed order results computed as described in the text. The scale is $Q = 10$ GeV. (For interpretation of the references to colour in this figure legend, the reader is referred to the web version of this article.)

where $\Sigma^B_{\gamma \mathrm{h}}(\rho, m_B)$ is the cross-section computed using resummation, and $\Sigma^O_{\gamma \mathrm{h}}(\rho, m_B)$ the cross-section computed using the same gluon distribution, but with the LO hard cross-section (which here is simply $C(0,0) = \frac{7\pi}{9} e_Q^2 \alpha\alpha_s$, i.e. the first term in the expansion (3.24)). To calculate $\Sigma^B_{\gamma \mathrm{h}}$ we use the same techniques as in the previous section: poles at $M = 1$ are dealt with using the exponentiation trick (3.11), while powers are turned into derivatives according to (3.4): the only new feature is that each term gets multiplied by the various coefficients in (3.24), (3.25), or (3.26). The results are plotted in Fig. 10: the blue curves are the resummed results computed using the three approximations (3.24), (3.25), and (3.26). The results are indistinguishable on the plot, and thus may be taken to be the exact result: as in the previous calculation, the Taylor series is an adequate approximation to the more accurate pole approximations (3.25) and (3.26) for all $\rho \gtrsim 10^{-10}$.

Also in Fig. 10 we plot the K-factors for fixed order perturbation theory, at NLO, NNLO and NNNLO. Note that these are computed with the GLAP gluon distributions at the appropriate order (LO, NLO and NNLO), not with the resummed distribution. To do these calculations we use the result Eq. (2.27) to evaluate the dominant contributions to the fixed order hard cross-section: these are $O(\frac{\alpha_s}{N})$ at NLO (these are the terms computed in [36], not the full result of Ref. [37]), $O(\frac{\alpha_s^2}{N^2})$ and $O(\frac{\alpha_s^2}{N})$ at NNLO, and $O(\frac{\alpha_s^3}{N^3})$, $O(\frac{\alpha_s^3}{N^2})$, and $O(\frac{\alpha_s^2}{N})$ at NNNLO. They may thus be computed using the $O(M)$, $O(M^2)$ and $O(M^3)$ terms in the Taylor expansion (3.24) provided we use at least the LO, NLO and NNLO results respectively for the evolved gluon distributions. It may be seen from the plot that while the NLO calculation seriously underestimates the K-factor for $\rho \lesssim 10^{-4}$, the NNLO calculation is fine down to $\rho \sim 10^{-8}$, while the NNNLO

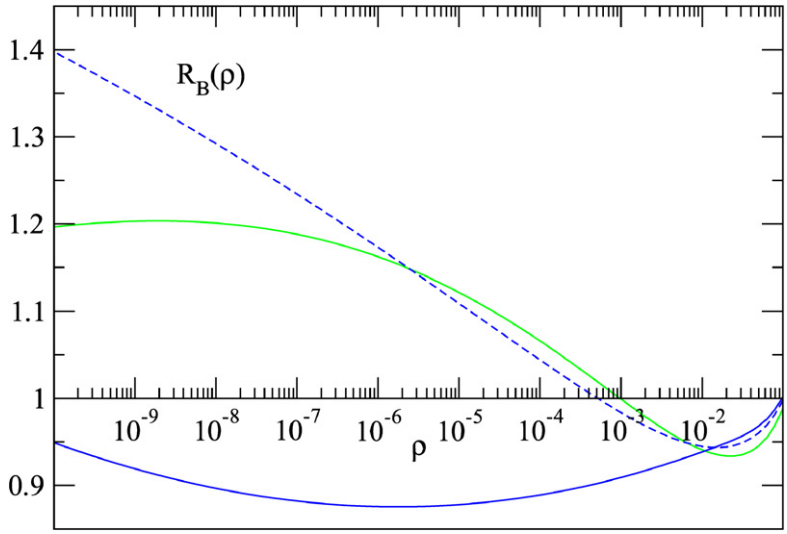

Fig. 11. The resummation factor R_B for photoproduction. The solid blue (lower) curve includes resummation in both evolution and hard cross-section, while the dashed blue curve only has resummation in the cross-section. The green (upper) curve is the same computation comparing NNLO to NLO perturbation theory. (For interpretation of the references to color in this figure legend, the reader is referred to the web version of this article.)

is worse, starting to overshoot below 10^{-7} or so. So it seems that while a NLO calculation of the hard cross-section is inadequate at high energy, a NNLO calculation can perform well, the fully resummed result being only really necessary at very small values of ρ.

To explore the relative sizes of the various resummation contributions, in Fig. 11 we plot the "resummation factor" for photoproduction of $b\bar{b}$ pairs:

$$R_B(\rho) = \frac{\Sigma^B_{\gamma\mathrm{h}}(\rho, m_B)}{\Sigma^{\mathrm{NLO}}_{\gamma\mathrm{h}}(\rho, m_B)}, \tag{3.28}$$

where $\Sigma^B_{\gamma\mathrm{h}}$ is computed as previously, while $\Sigma^{\mathrm{NLO}}_{\gamma\mathrm{h}}$ is computed using the NLO hard cross-section and NLO GLAP gluon distribution. The result is the solid blue curve: the net effect of the resummation is to reduce the cross-section by between 5% and 10%, rather uniformly over the full range of ρ. The dashed blue curve is the same calculation but with $\Sigma^B_{\gamma h}$ computed using the NLO GLAP gluon, rather than the resummed one, to assess the relative effects of the resummation of the cross-section and the resummation of the evolved gluon: clearly both effects are of similar importance, since when combined they almost cancel. The green curve is the ratio $\Sigma^{\mathrm{NNLO}}_{\gamma\mathrm{h}}/\Sigma^{\mathrm{NLO}}_{\gamma\mathrm{h}}$, with $\Sigma^{\mathrm{NNLO}}_{\gamma\mathrm{h}}$ computed with a consistent NNLO cross-section and gluon, for comparison with the resummed result: from this it is clear that a full NNLO calculation does not give a good approximation to the resummed cross-section for $\rho \lesssim 10^{-2}$, despite giving a good account of the hard cross-section. This is because the NNLO evolution is not very close to the resummed evolution, as it underestimates the suppression [12]. Taken together, these three curves probably give a reasonable impression of the overall range of uncertainty in the $b\bar{b}$-photoproduction cross-section at high energy.

4. Hadroproduction

4.1. The gluon–gluon luminosity

When we calculate hadronic cross-sections, using the factorization (2.2) or equivalently (2.14), it is convenient to first define the gluon–gluon luminosity density[3]

$$\begin{aligned} L_z(z,Q_1,Q_2) &= \int_\rho^1 \frac{dx_1}{x_1}\int_\rho^1 \frac{dx_2}{x_2}\delta(z-x_1x_2)G(x_1,Q_1)G(x_2,Q_2)\\ &= \int_z^1 \frac{dy}{y}G\left(\frac{z}{y},Q_1\right)G(y,Q_2)\\ &= \int_{-i\infty}^{i\infty}\frac{dN}{2\pi i}e^{\xi N}\int_{-i\infty}^{i\infty}\frac{dM_1}{2\pi i}\frac{dM_2}{2\pi i}e^{t_1M_1+t_2M_2}G(N,M_1)G(N,M_2), \end{aligned} \tag{4.1}$$

where $\xi=\ln 1/z$, $t_1=\ln Q_1^2/\Lambda^2$, $t_2=\ln Q_2^2/\mu^2$. Thus we have in Mellin space simply

$$L_z(N,M_1,M_2)=G(N,M_1)G(N,M_2), \tag{4.2}$$

so Eq. (2.14) reads

$$\begin{aligned} \Sigma_{\rm hh}(\rho,Q) &= \int_{-i\infty}^{i\infty}\frac{dN}{2\pi i}e^{\xi N}\int_{-i\infty}^{i\infty}\frac{dM_1}{2\pi i}\frac{dM_2}{2\pi i}e^{t(M_1+M_2)}H(N,M_1,M_2)L_z(N,M_1,M_2)\\ &= \int_\rho^1\frac{dz}{z}\int\frac{d^2\mathbf{k}_1}{\pi\mathbf{k}_1^2}\int\frac{d^2\mathbf{k}_2}{\pi\mathbf{k}_2^2}\Sigma_{gg}\left(\frac{\rho}{z},\frac{\mathbf{k}_1}{Q},\frac{\mathbf{k}_2}{Q}\right)L_z\left(z,\mathbf{k}_1^2,\mathbf{k}_2^2\right), \end{aligned} \tag{4.3}$$

where now we have set $t_1=t_2=t=\ln Q^2/\Lambda^2$, Q being the invariant mass in the final state. Substituting (4.1) into (4.3) then gives back the gluon–gluon contribution to (2.2), as it should.

It is straightforward to compute $L_z(\rho,Q,Q)\equiv L_z(\rho,Q)$ from the gluon distribution $G(x,Q)$ shown in Fig. 4: the result is show in Fig. 12. Note that the luminosity only starts to rise at large Q when $\rho\lesssim 10^{-5}$ or so, whereas for the gluon distribution the rise sets in already at $x\sim 10^{-3}$. Again the resummed luminosity grows rather more slowly under the resummed evolution than with NLO GLAP evolution.

Of course in a hadron collider it is not always possible to vary ρ and Q independently as one does in photoproduction: the inclusive cross-section for the hadroproduction of a final state of invariant mass Q depends instead on $L_z(Q)\equiv L_z(Q^2/S,Q,Q)$, where S is the (fixed) centre-of-mass energy of the machine. This is plotted in Fig. 13 for three different colliders: the Tevatron, the LHC, and a notional VLHC with $\sqrt{S}=200$ TeV. Note that $Q^{-1}L_z(Q)$ gives a rough estimate of the inclusive cross-section.

[3] In the literature it is more usual to call this quantity $d\mathcal{L}/d\tau$, where $\tau=x_1x_2$: after integration $\mathcal{L}$ is then the total gluon–gluon luminosity.

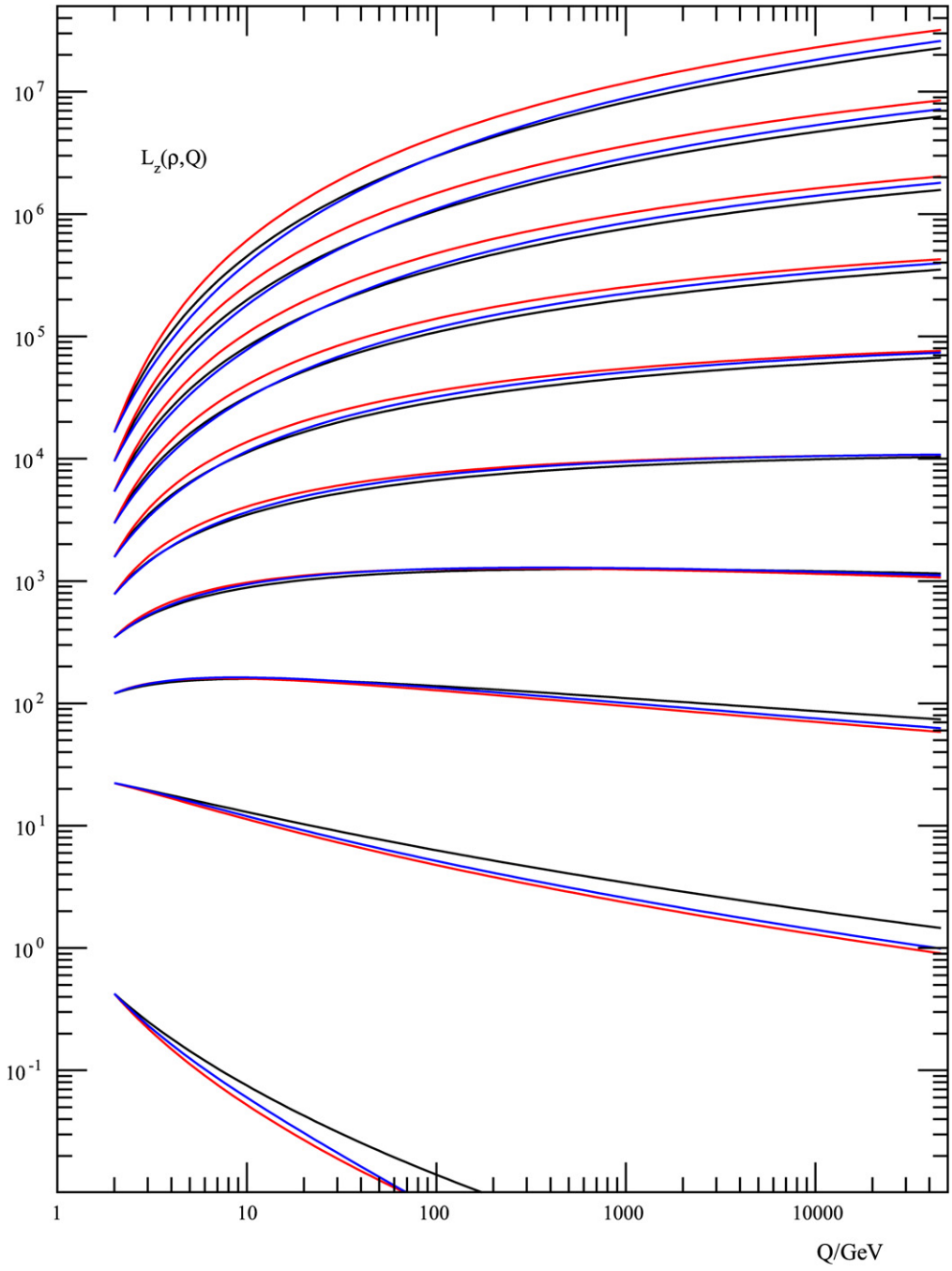

Fig. 12. The gluon–gluon luminosity density $L_z(\rho, Q)$ plotted against Q in GeV for $\rho = 10^{-10}, 10^{-9}, \ldots, 0.01, 0.1$ (from top to bottom). The blue curves are evolved with the NLO resummation described in the text: the black and red curves are with LO and NLO GLAP evolution. (For interpretation of the references to colour in this figure legend, the reader is referred to the web version of this article.)

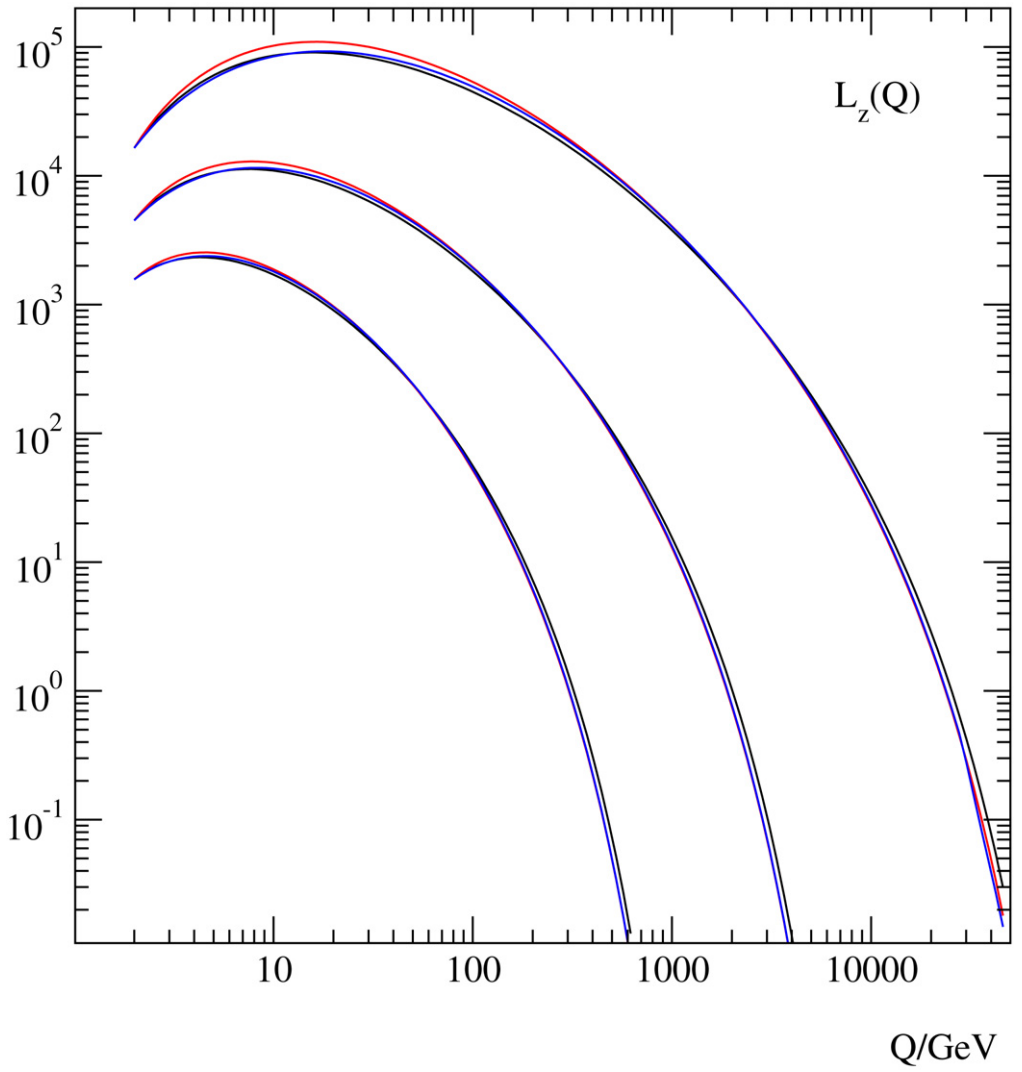

Fig. 13. The gluon–gluon luminosity $L_z(Q)$ plotted against the invariant mass Q in GeV. The lower curves are for the Tevatron, the middle curves for LHC, and the upper for a VLHC: the colour coding is the same as in Fig. 12. (For interpretation of the references to colour in this figure legend, the reader is referred to the web version of this article.)

4.2. Resumming the dominant infrared singularity

In order to compute the inclusive cross-section Eq. (4.3) we must first compute the hard cross-section, and then convolute it with the gluon–gluon luminosity. In practice this means we must perform the inverse Mellin transforms over N, M_1 and M_2. Since all the collinear and high energy logarithms are already included in the luminosity, the hard cross-section $H(N, M_1, M_2)$ is regular at $N = M_1 = M_2 = 0$, and we may Taylor expand it using (2.24). Just as in the photoproduction case Eq. (3.4), the resulting integrals over powers of M_1 and M_2 may then be evaluated in terms of derivatives of the luminosity: writing $L_z(N, t) \equiv L_z(N, t, t)$ for simplicity, then for

all $m_1, m_2 = 0, 1, 2, \ldots$

$$\int_{-i\infty}^{i\infty} \frac{dM_1}{2\pi i}\frac{dM_2}{2\pi i} e^{t(M_1+M_2)} M_1^{m_1} M_2^{m_2} L_z(N, M_1, M_2) = \frac{\partial^{m_1+m_2}}{\partial t_1^{m_1}\partial t_2^{m_2}} L_z(N, t_1, t_2)\Big|_{t_1=t_2=t}. \tag{4.4}$$

The derivatives of the luminosity are then given in turn by

$$\begin{aligned}
&\frac{\partial}{\partial t_1} L_z(N, t_1, t_2)\Big|_{t_1=t_2=t} = \frac{\partial}{\partial t_2} L_z(N, t_1, t_2)\Big|_{t_1=t_2=t} = \gamma(N, t) L_z(N, t),\\
&\frac{\partial^2}{\partial t_1^2} L_z(N, t_1, t_2)\Big|_{t_1=t_2=t} = \frac{\partial^2}{\partial t_2^2} L_z(N, t_1, t_2)\Big|_{t_1=t_2=t} = \left(\gamma^2 + \dot{\gamma}\right) L_z(N, t),\\
&\frac{\partial^2}{\partial t_1 \partial t_2} L_z(N, t_1, t_2)\Big|_{t_1=t_2=t} = \gamma^2 L_z(N, t),\\
&\frac{\partial^3}{\partial t_1^3} L_z(N, t_1, t_2)\Big|_{t_1=t_2=t} = \frac{\partial^3}{\partial t_2^3} L_z(N, t_1, t_2)\Big|_{t_1=t_2=t} = \left(\gamma^3 + 3\gamma\dot{\gamma} + \ddot{\gamma}\right) L_z(N, t),\\
&\frac{\partial^3}{\partial t_1^2 \partial t_2} L_z(N, t_1, t_2)\Big|_{t_1=t_2=t} = \frac{\partial^3}{\partial t_1 \partial t_2^2} L_z(N, t_1, t_2)\Big|_{t_1=t_2=t}\\
&\qquad = \left(\gamma^3 + \gamma\dot{\gamma}\right) L_z(N, t), \ldots.
\end{aligned} \tag{4.5}$$

The first two of these are plotted in Fig. 14 (to be compared with Fig. 8): again even the first derivative is below unity for all except the smallest values of ρ and Q, and the second derivative is considerably smaller than the first. The resummed derivatives are smaller at small ρ and Q than the corresponding GLAP derivatives. Given these facts, we expect the first few terms of the Taylor series to give a good approximation to the full cross-section at all except the highest energies and lowest scales, just as they did in photoproduction.

It remains to consider the singularities of the hard cross-section (see Fig. 15). Just as in the photoproduction case there will be higher twist singularities at $M_1, M_2 = -1, -2, -3, \ldots$ which will lead to terms suppressed by inverse powers of the hard scale Q^2: these will not concern us here. The structure of the infrared singularities is more subtle: there are singularities at $M_1, M_2 = 1, 2, 3, \ldots$ just as in photoproduction, but there are now also infrared singularities on the lines $M_1 + M_2 = 1, 2, 3, \ldots$, as discussed in Section 2.6. Since these come closest to the origin, it is likely that they dominate at high energies, and indeed as we shall see this turns out to be the case.

In order to integrate over the line of poles at $M_1 + M_2 = 1$, we may employ the same trick that we used for the $M = 1$ pole in Section 3.2:

$$\frac{1}{(1 - M_1 - M_2)^n} = \frac{1}{n!}\int_0^\infty d\tau\, \tau^{n-1} e^{-\tau(1-M_1-M_2)} \tag{4.6}$$

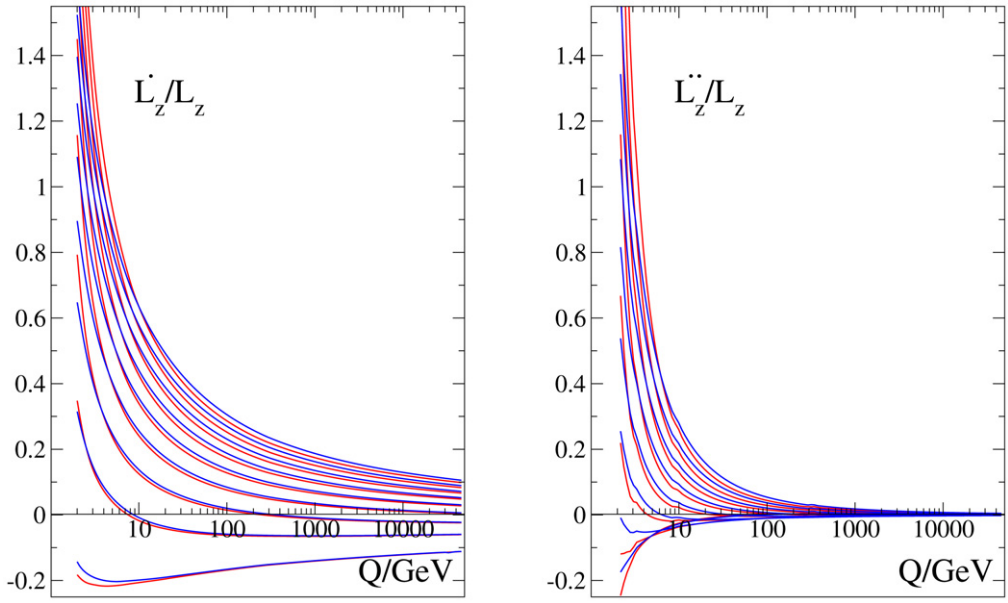

Fig. 14. The first (left) and second (right) derivatives with respect to $t = \ln Q^2/\Lambda^2$ of the gluon–gluon luminosity $L_z(\rho, Q)$ plotted in Fig. 13, normalised to L_z, plotted against Q in GeV, for $\rho = 10^{-10}, 10^{-9}, \ldots, 0.01$ (from top to bottom). Again the blue curves are with NLO resummed evolution, the red with NLO GLAP evolution.

for $n = 1, 2, \ldots$. The nice extra feature here is that under the integral over τ the dependence on M_1 and M_2 has now factorised, allowing both integrals to be performed independently:

$$\begin{aligned}\Sigma^n_{\rm hh}(N,t) &= \int_{-i\infty}^{i\infty} \frac{dM_1}{2\pi i}\frac{dM_2}{2\pi i}\frac{1}{(1-M_1-M_2)^n} e^{t(M_1+M_2)} G(N,M_1)G(N,M_2)\\ &= \frac{1}{n!}\int_0^\infty d\tau\, \tau^{n-1}e^{-\tau} \int_{-i\infty}^{i\infty}\frac{dM_1}{2\pi i} e^{(t+\tau)M_1} G(N,M_1) \int_{-i\infty}^{i\infty}\frac{dM_2}{2\pi i} e^{(t+\tau)M_2} G(N,M_2)\\ &= \frac{1}{n!}\int_0^\infty d\tau\, \tau^{n-1}e^{-\tau} L_z(N,t+\tau), \end{aligned} \tag{4.7}$$

where in the last line we have exploited the factorization to perform both of the integrals over M_1 and M_2, writing the result in terms of the gluon–gluon luminosity $L_z(N,t)$. In this way we reduce a double integral over two complex variables with a line of singularity to a single real integral, which clearly converges rather rapidly when the coupling runs since $L_z(N,t)$ is very smooth (see Fig. 12). Again where $L_z(\rho, Q)$ increases monotonically in Q the singularity will give an enhancement of the cross-section, which will be most significant when the rise is steepest (i.e. small ρ and low Q).

It is easy to see that the same arguments used for the photoproduction and electroproduction cross-sections, in particular (3.14) and (3.15), will also apply here, because of the factorization under the τ integral in (4.7). Thus when the coupling runs the line singularity is once

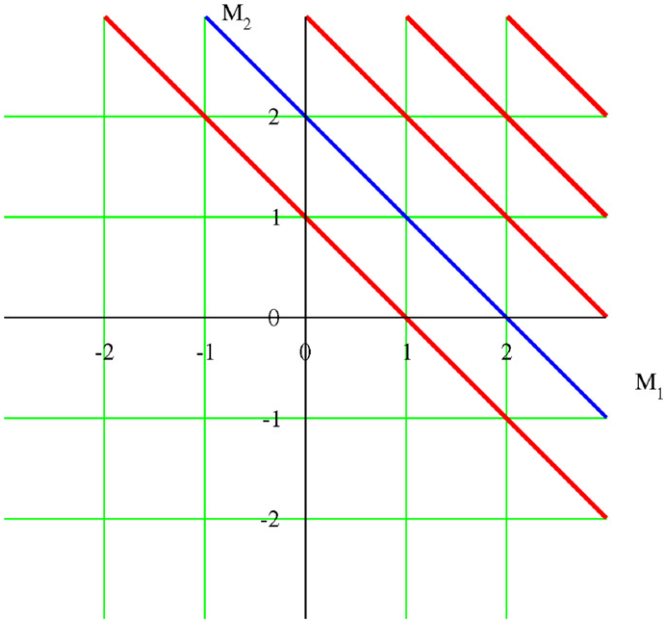

Fig. 15. A schematic picture of the location of the singularities of a hadroproduction impact factor $H(0, M_1, M_2)$ in the M_1–M_2 plane. The particular singularities shown are those for heavy quark production: those in green (parallel to the axes) are simple poles, in blue double poles and in red triple poles (diagonal). (For interpretation of the references to colour in this figure legend, the reader is referred to the web version of this article.)

again pushed to infinity, and the only singularities of $\Sigma^n_{\rm hh}(N,t)$ in the N-plane are those of the anomalous dimension $\gamma(N,t)$. The running of the coupling thus ensures that all infrared singularities, whether in the evolution or in the hard cross-section, are factorised into the initial (non-perturbative) gluon distribution. An important consequence of this factorization is that the asymptotic high energy behaviour of inclusive hadroproduction cross-sections is determined entirely by the rise in the gluon distributions, just as it was in electroproduction and photoproduction. It follows that the high energy powerlike rise due to the rightmost singularity in the anomalous dimension is universal: all inclusive cross-sections rise in the same way.

To see how well all this works in practice, consider a triple pole, i.e. $n = 3$, and define the K-factor as the ratio

$$K_3(Q) = \frac{\Sigma^3_{hh}(Q^2/S, Q)}{\Sigma^0_{hh}(Q^2/S, Q)}, \tag{4.8}$$

where the denominator $\Sigma^0_{hh}(Q^2/S, Q)$ is simply the gluon–gluon luminosity distribution $L_z(\xi, t)$ when $\xi = \ln S/Q^2$. Then

$$K_3(Q) = \frac{1}{L_z(\xi,t)} \int_{-i\infty}^{i\infty} \frac{dN}{2\pi i} e^{N\xi} \int_0^\infty d\tau\, \tau^2 e^{-\tau} L_z(N, t+\tau) \tag{4.9}$$

$$= 1 + \frac{3}{L_z(\xi,t)}\frac{\partial}{\partial t}L_z(\xi,t) + \frac{6}{L_z(\xi,t)}\frac{\partial^2}{\partial t^2}L_z(\xi,t) + \frac{10}{L_z(\xi,t)}\frac{\partial^3}{\partial t^3}L_z(\xi,t) + \cdots, \tag{4.10}$$

where in the first line we used (4.7), and in the second we Taylor expand $L_z(N,t+\tau)$ and integrate term by term. The diagonal derivatives of the luminosity are readily deduced from (4.5):

$$\begin{aligned}
&\frac{\partial}{\partial t}L_z(N,t) = 2\gamma(N,t)L_z(N,t),\\
&\frac{\partial^2}{\partial t^2}L_z(N,t) = 2\bigl(2\gamma^2+\dot\gamma\bigr)L_z(N,t),\\
&\frac{\partial^3}{\partial t^3}L_z(N,t) = 2\bigl(4\gamma^3+6\gamma\dot\gamma+\ddot\gamma\bigr)L_z(N,t),\ldots.
\end{aligned} \tag{4.11}$$

Using the resummed luminosity distribution shown in Fig. 12 it is now a simple matter to compute the K-factor, using either (4.9) or the series (4.10). The results are shown in Fig. 16, for $S = 2$ TeV, 14 TeV and 200 TeV. At sufficiently low invariant mass Q and thus large ρ the K factor rises steeply as expected, eventually resulting in very large corrections. In each case the exact result (4.9) is well approximated by only the first few terms in (4.10). In fact above $Q \sim 5$ GeV at the Tevatron, $Q \sim 15$ GeV at the LHC and $Q \sim 70$ GeV at a VLHC the $O(M)$ (i.e. NLO) correction alone already gives a good approximation: only below these scales do the $O(M^2)$ (NNLO) corrections become significant. The NNLO approximation only really starts to be inadequate when $Q \lesssim 5$ GeV at the VLHC, which would no doubt be outside the range of acceptance

These results are interesting because, as shall show explicitly for heavy quark production in the next section, the line of triple poles (2.32) is sufficiently singular to provide the dominant contribution to the cross-section. Moreover since these infrared singularities are quite generic, we expect other inclusive cross-sections such as the inclusive jet cross-section to acquire K-factors at high energy similar to those shown in Fig. 16. Calculation of the K-factor can then proceed in each case through a computation of the expansion of the hard cross-section $H(N, M_1, M_2)$ in M_1 and M_2, i.e. by perturbation about the on-shell result: the singularity will then generate large coefficients of the $O(M_1 + M_2)$ and $O((M_1 + M_2)^2)$ terms, and thus large NLO and (at high enough energy) NNLO K-factors.

This mechanism thus provides a simple explanation for the large K-factors commonly found in hadroproduction processes at high energy. Constraining the incoming gluons to be on-shell as in the usual LO calculation keeps the timelike intermediate gluon in Fig. 6(b) or Fig. 7(b) away from its mass-shell. Releasing this constraint either by using the off-shell formalism used here, or by going to higher order in α_s in the more usual on-shell formalism (with in particular contributions from diagrams in which one (NLO) or both (NNLO) incoming gluons emits another gluon), allows the intermediate gluon to get close to its mass-shell, and thus produces the large enhancements evident in Fig. 16.

To test this idea it is instructive to compare the resummed K-factors with those computed in fixed order-perturbation theory. At high energy this is easily done by using the expansion (4.10), applied to the luminosity evolved using GLAP evolution (at LO for the NLO K-factor, NLO for the NNLO, and NNLO for the NNNLO), just as we did for photoproduction in Fig. 10: the results are shown in Fig. 17. At the Tevatron NLO GLAP perturbation theory for the hard cross-section does pretty well except at very low scales (appropriate for charm production). At LHC NNLO is starting to be important already around the beauty threshold, while at a VLHC NLO

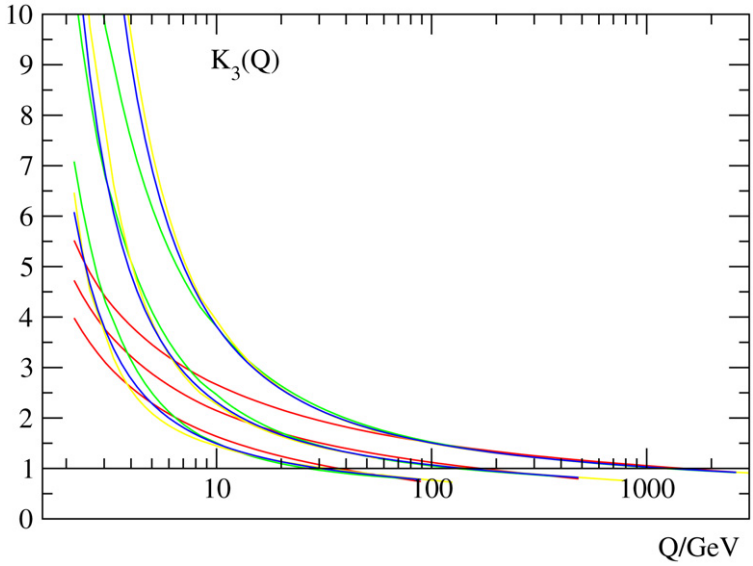

Fig. 16. A generic hadroproduction K-factor for a triple pole $1/(1 - M_1 - M_2)^3$, plotted against invariant mass Q, for three different colliders: the Tevatron (lower curves), the LHC (middle curves) and a VLHC (upper curves). In each case the blue (upper) lines correspond to the exact expression Eq. (4.9), while the red, green and yellow (bottom to top) lines are the NLO, NNLO and NNNLO approximation to it computed by including the second, third and fourth terms respectively of the series (4.10). (For interpretation of the references to colour in this figure legend, the reader is referred to the web version of this article.)

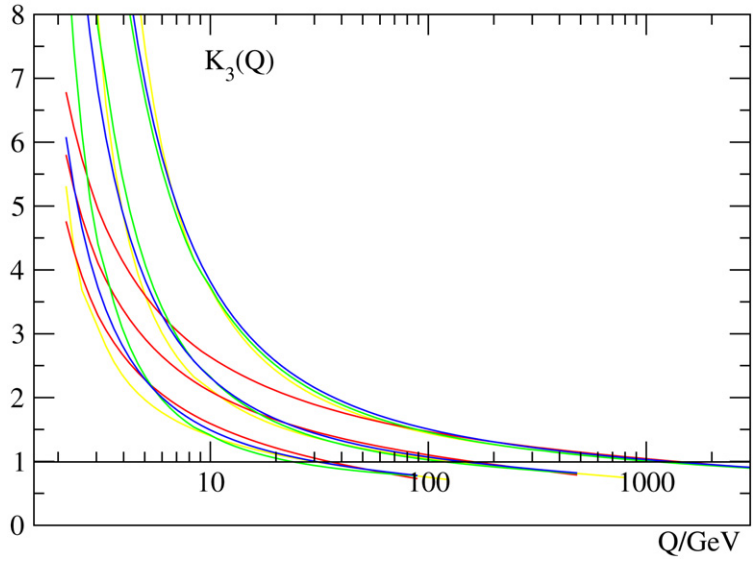

Fig. 17. The same as Fig. 16, except that now the red, green and yellow lines are the NLO, NNLO and NNNLO results in fixed order perturbation theory (at high energy), computed by including the second, third and fourth terms respectively of the series (4.10), with the luminosity evolved using GLAP evolution at the appropriate order.

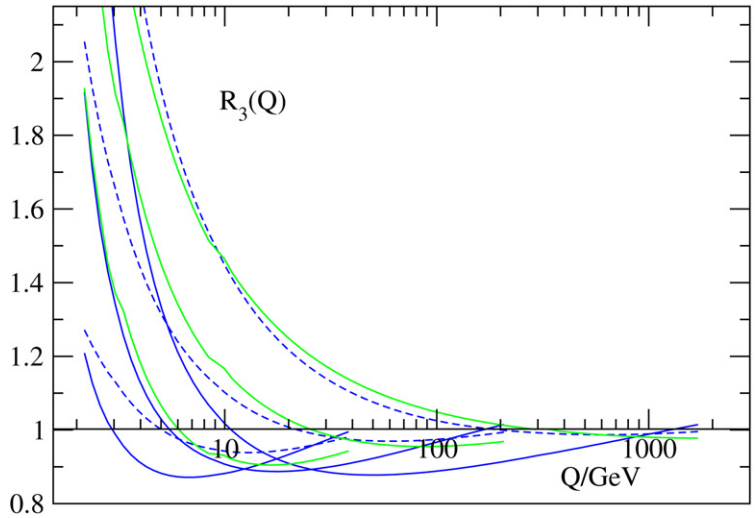

Fig. 18. The resummation factor R_3 for a generic hadroproduction process. As in Fig. 11 the solid blue (lower) curve includes resummation in both evolution and hard cross-section, while the dashed blue curve only has resummation in the cross-section. The green (upper) curve compares NNLO to NLO unresummed perturbation theory. (For interpretation of the references to colour in this figure legend, the reader is referred to the web version of this article.)

is only good at scales above 60 GeV. For beauty production at VLHC the NNLO correction is very large—around 50% above NLO. More importantly, the NNNLO correction is nowhere an improvement on the NNLO result: beyond NNLO the resummed result is more useful.

To assess the impact of the resummation, in Fig. 18 we plot the "resummation factor"

$$R_3^h(Q) = \frac{\Sigma_{hh}^3(Q^2/S, Q)}{\Sigma_{hh}^{\rm NLO}(Q^2/S, S)}, \tag{4.12}$$

where, as in Eq. (3.28), the reference cross-section $\Sigma_{hh}^{\rm NLO}$ is computed using the NLO hard cross-section and NLO GLAP gluon distribution. Again we have a substantial cancellation between the suppression of the luminosity due to the resummation of the evolution and the enhancement of the cross-section due to the triple pole in the hard cross-section. At intermediate scales ($Q \sim$ 8, 20, 60 GeV for Tevatron, LHC and VLHC respectively) the resummation gives an overall suppression of around 10%: below these scales the suppression starts to turn into an enhancement due to the rapidly rising partonic cross-section. However these enhancements are generally at scales sufficiently small that they would escape detection in all but a very forward detector. Again we also show the ratio of the NNLO to NLO fixed order computation: this overestimates the cross-section because it underestimates the suppression of the gluon–gluon luminosity due to resummation.

4.3. Hadroproduction of heavy quarks

As a specific example of resummation in hadroproduction we now consider the hadroproduction of heavy quarks, specifically $b\bar{b}$-production at the Tevatron, LHC and VLHC. The LO contribution to the hard cross-section then involves the computation of the two diagrams in Fig. 6 with both incoming gluons taken off-shell. Unlike the photoproduction cross-section Eq. (3.21)

the hadroproduction cross-section has been evaluated analytically only in the high energy limit $N = 0$: the result is the impact factor [16,27][4]

$$\begin{aligned}
&H(0, M_1, M_2)\\
&\quad = \alpha_s^2 \frac{\pi}{N_c^2 - 1} \Gamma(1 + M_1)\Gamma(1 - M_1)\Gamma(1 + M_2)\Gamma(1 - M_2)\\
&\qquad \times \left[4N_c \frac{(\Gamma(3 - M_1 - M_2))^2}{(1 - M_1 - M_2)\Gamma(6 - 2(M_1 + M_2))} \left(1 + \left(\frac{\Gamma(1 - M_1 - M_2)}{\Gamma(1 - M_1)\Gamma(1 - M_2)} \right)^2 \right) \right.\\
&\qquad \left. - \frac{2}{N_c} \big(7 - 5(M_1 + M_2) + 3M_1 M_2\big) \frac{\Gamma(2 - M_1)\Gamma(2 - M_2)\Gamma(1 - M_1 - M_2)}{\Gamma(4 - 2M_1)\Gamma(4 - 2M_2)} \right].
\end{aligned} \tag{4.13}$$

The second term in this expression is due solely to the "Abelian" diagram Fig. 6(a): when one leg is on-shell (e.g. $M_2 = 0$ and $M_1 = M$) this term reduces to $C(0, M)$ Eq. (3.22) up to an overall constant vertex factor. The first term is due to the intrinsically non-Abelian diagram Fig. 6(b): it is this piece which contains the triple pole singularity (2.32), which dominates the cross-section at high energy.

Consider the structure of the result Eq. (4.13) in various regions of the M_1–M_2 plane Fig. 15. It has higher twist (simple) poles at $M_1, M_2 = -1, -2, \ldots$, and infrared (anti-collinear) poles at $M_1, M_2 = 1, 2, \ldots$: for example near $M_1 = 1$

$$H(0, M_1, M_2) \sim \alpha_s^2 \frac{4\pi}{N_c} \left[\frac{1}{1 - M_1} \frac{\Gamma(M_2)\Gamma(1 - M_2)(\Gamma(2 - M_2))^2}{\Gamma(4 - 2M_2)} + O(1) \right], \tag{4.14}$$

thus a simple pole except when M_2 is an integer, at which special points there is a double pole. However it also has lines of singularity when $M_1 + M_2 = 1, 2, \ldots$: writing $M_\pm \equiv M_1 \pm M_2$, the Laurent expansion about $M_+ = 1$ is

$$\begin{aligned}
&H(0, M_1, M_2)\\
&\quad \sim \alpha_s^2 \frac{\pi}{N_c^2 - 1} \left[\frac{N_c}{6} \frac{1 - M_-^2}{(1 - M_+)^3} \right.\\
&\qquad + \frac{1}{(1 - M_+)^2} \frac{N_c}{18} \left(3\big(1 - M_-^2\big) \left(2\psi(1) - \psi\left(\frac{1}{2} + \frac{1}{2} M_- \right) - \psi\left(\frac{1}{2} - \frac{1}{2} M_- \right) \right) \right.\\
&\qquad \left. \left. - 11 + 5M_-^2 \right) \right.\\
&\qquad \left. - \frac{1}{1 - M_+} \left(\frac{(67 + 72(\ln 2)^2 - 132 \ln 2) N_c}{54} - \frac{11\pi^3}{384 N_c} + O\big(M_-^2\big) \right) + O(1) \right],
\end{aligned} \tag{4.15}$$

i.e. triple, double and simple poles, except again at the special points $M_- = \pm 1$ (and thus $(M_1, M_2) = (1, 0)$ or $(0, 1)$) where the triple pole reduces to a double pole, the double to a single.

For M_1 and M_2 close to zero the impact factor is regular, as it must be, with Taylor expansion

[4] In Refs. [15,16,27] the function $H(N, M_1, M_2)$ is denoted by $h_\omega(\gamma_1, \gamma_2)$.

$$
\begin{aligned}
&H(0,M_1,M_2)\\
&\quad=\alpha_s^2\frac{\pi}{N_c^2-1}\Bigg[\left(\frac{4N_c}{15}-\frac{7}{18N_c}\right)+\left(\frac{154N_c}{225}-\frac{41}{54N_c}\right)(M_1+M_2)\\
&\qquad+\left(\frac{4924N_c}{3375}-\frac{122}{81N_c}\right)\left(M_1^2+M_2^2\right)\\
&\qquad+\left(\frac{(9848-150\pi^2)N_c}{3375}-\frac{(470+21\pi^2)}{324N_c}\right)M_1M_2\\
&\qquad+\left(\frac{(150544-27000\zeta_3)N_c}{50625}-\frac{(730-189\zeta_3)}{243N_c}\right)\left(M_1^3+M_2^3\right)\\
&\qquad+\Bigg(\frac{(150544-22500\zeta_3-1925\pi^2)N_c}{16875}\\
&\qquad-\frac{(2776+378\zeta_3+123\pi^2)}{972N_c}\Bigg)(M_1+M_2)M_1M_2+O\left(M^4\right)\Bigg]\\
&\quad\simeq 0.2633\alpha_s^2\Big(1+2.69(M_1+M_2)+5.78(M_1+M_2)^2-1.50M_1M_2\\
&\qquad+9.41(M_1+M_2)^3-2.79(M_1+M_2)M_1M_2+O\left(M^4\right)\Big).
\end{aligned}
\tag{4.16}
$$

The rather large numerical coefficients in this expansion (compare them to those of the expansion (3.24)), in particular of the powers of M_1+M_2, are due to the dominance of the nearby triple pole singularity (4.15): if we first subtract the triple pole, and then Taylor expand what is left, we find

$$
\begin{aligned}
&H(0,M_1,M_2)\\
&\quad\simeq\alpha_s^2\frac{\pi}{N_c^2-1}\Bigg[\frac{N_c}{6}\frac{1}{(1-M_1-M_2)^3}+\left(\frac{N_c}{10}-\frac{7}{18N_c}\right)\\
&\qquad+\left(\frac{83N_c}{450}-\frac{41}{54N_c}\right)(M_1+M_2)+\left(\frac{1549N_c}{3375}-\frac{122}{81N_c}\right)\left(M_1^2+M_2^2\right)\\
&\qquad+\left(\frac{(3098-150\pi^2)N_c}{3375}-\frac{(470+21\pi^2)}{324N_c}\right)M_1M_2\\
&\qquad+\left(\frac{(66169-27000\zeta_3)N_c}{50625}-\frac{(730-189\zeta_3)}{243N_c}\right)\left(M_1^3+M_2^3\right)\\
&\qquad+\left(\frac{(66169-22500\zeta_3-1925\pi^2)N_c}{16875}-\frac{(2776+378\zeta_3+123\pi^2)}{972N_c}\right)\\
&\qquad\times(M_1+M_2)M_1M_2+O\left(M^4\right)\Bigg]\\
&\quad\simeq 0.2633\alpha_s^2\Bigg(\frac{0.74591}{(1-M_1-M_2)^3}+0.2541+0.448(M_1+M_2)+1.31(M_1+M_2)^2\\
&\qquad-1.50M_1M_2+1.95(M_1+M_2)^3-2.79(M_1+M_2)M_1M_2+O\left(M^4\right)\Bigg).
\end{aligned}
\tag{4.17}
$$

A further reduction in the coefficients may be obtained by also subtracting the double pole.

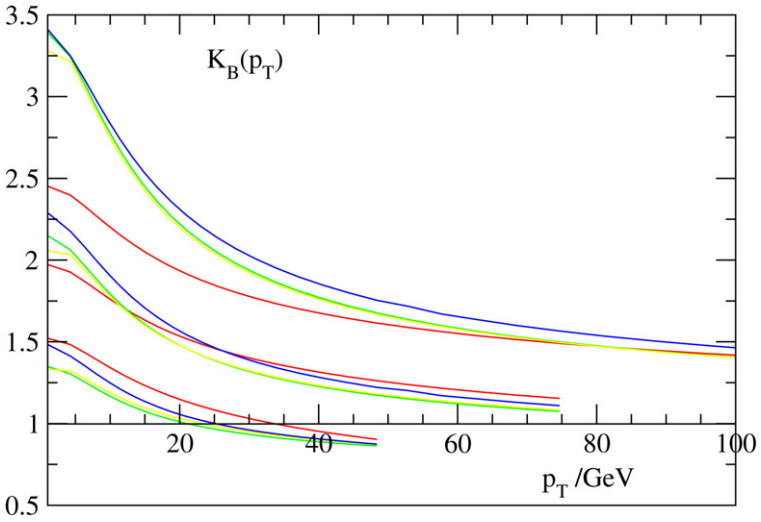

Fig. 19. The K-factor for hadroproduction of $b\bar{b}$ pairs as a function of their minimum p_T, at the Tevatron (lower), LHC (middle) and VLHC (upper). As in Fig. 17 the blue curves are the resummed result, while the red green and yellow curves are fixed order perturbation theory at NLO, NNLO and NNNLO respectively, computed as described in the text.

It is now straightforward to compute the hadronic cross-sections using either the Taylor expansion (4.16) or the more precise expansion (4.17), the expressions (4.4) and (4.5) for the powers of M_1 and M_2, the representation (4.7) for the triple pole in (4.17), and the gluon–gluon luminosity shown in Fig. 12. The results are presented in Fig. 19 as a K-factor

$$K_B(p_T) = \left.\frac{\Sigma^B_{hh}(Q^2/S, Q)}{\Sigma^0_{hh}(Q^2/S, Q)}\right|_{Q^2=m_B^2+p_T^2}, \tag{4.18}$$

where Σ^B_{hh} is the fully resummed calculation, and the reference cross-section Σ^0_{hh} is evaluated using $H(0,0,0) = \alpha_s^2 \frac{181\pi}{2160}$, thus dividing out the overall normalization and the primary dependence on the gluon–gluon luminosity. Both cross-sections are evaluated at $Q^2 = m_B^2 + p_T^2$, where p_T is its minimum average transverse momentum of the $b\bar{b}$ pair. Note that we do not compute the transverse momentum distribution (the hard cross-section $H(N, M_1, M_2)$ is fully inclusive): the p_T dependence of (4.18) is simply a reflection of the restriction of the phase space when we require a higher invariant mass in the final state. We expect this to be the dominant effect here.

As we found in the previous section the naive Taylor expansion (4.16) and the pole resummed expansion (4.17) give almost identical results throughout the entire kinematic range: the two resummed curves in Fig. 19 are indistinguishable. In fact the convergence is so rapid that only the $O(M)$ (NLO) and $O(M^2)$ (NNLO) terms in (4.16) are actually needed: NNNLO contributions would only become significant for charm at a VLHC.

For comparison we also show in Fig. 19 results for fixed order (GLAP) perturbation theory at NLO, NNLO, and NNNLO, computed using the high energy approximation (as in Fig. 17) by using GLAP evolution, and keeping only the $O(M)$, $O(M^2)$ and $O(M^3)$ terms respectively in (4.16). At the Tevatron both the resummation and the NNLO GLAP corrections to the partonic cross-section give a slight suppression, while at the LHC there is a modest enhancement, at least at low p_T. Only at the VLHC is there a substantial enhancement, and even there a fixed order NNLO calculation of the partonic cross-section would be quite sufficient.

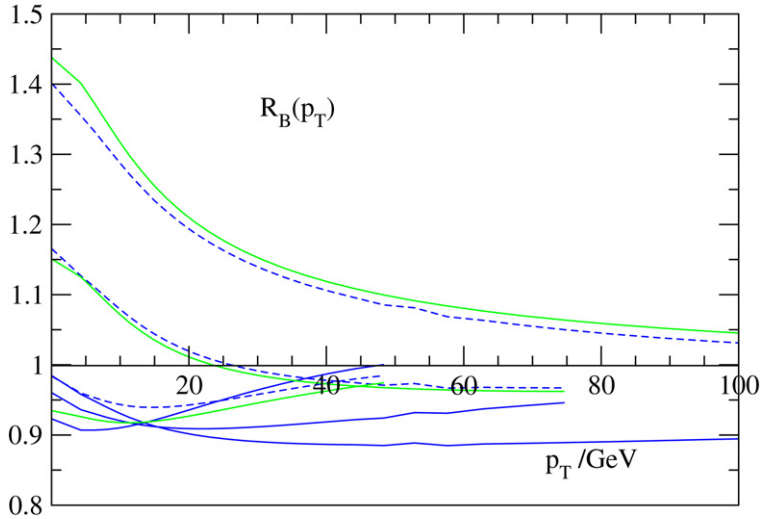

Fig. 20. The resummation factor R_B for a hadroproduction of $b\bar{b}$ pairs plotted against their transverse momentum. As in Fig. 18 the solid blue (lower) curve includes resummation in both evolution and hard cross-section, while the dashed blue curve only has resummation in the cross-section. The green (upper) curve is the same computation comparing NNLO to NLO perturbation theory. (For interpretation of the references to color in this figure legend, the reader is referred to the web version of this article.)

In order to estimate the overall effect of the resummation, we show in Fig. 20 the resummation factor

$$R_B(p_T) = \left.\frac{\Sigma^B_{hh}(Q^2/S, Q)}{\Sigma^{\rm NLO}_{hh}(Q^2/S, Q)}\right|_{Q^2=m_B^2+p_T^2}. \tag{4.19}$$

The reference cross-section is now the NLO fixed order cross-section computed with the NLO GLAP evolved gluon–gluon luminosity: unlike in the K-factor effects due to the different evolution of the luminosity are thus now included. As in Fig. 18 we find that the overall effect of the resummation is a net suppression by about 10%, which gradually goes away as p_T increases. Just above threshold this suppression is remarkably independent of the centre-of-mass energy S of the machine, and when this is very high (in particular for VLHC) the suppression goes away very slowly. So once again the enhancement expected from the triple pole in the cross-section is more than compensated by a suppression of the gluon–gluon luminosity.

It should be noted that all these calculations are only estimates: in particular a proper matching to the high ρ (Sudakov) region, inclusion of quark effects and realistic fitted parton distributions could all change the results substantially. In particular the suppression of the gluon–gluon luminosity by the resummation of the evolution is probably overestimated, since the starting distribution at 2 GeV is held fixed, rather than fitted to data. However the band between the upper and lower curves in Figs. 18 and 20 is probably a reasonable estimate of the current overall uncertainty due to resummation in hadroproduction cross-sections: for inclusive B production this means roughly $-5 \pm 5\%$ at the Tevatron, $5 \pm 10\%$ at the LHC and $20 \pm 20\%$ at a VLHC. In all cases it is probably comparable to the impact of NNLO in the partonic cross-section, and may result in a net suppression rather than an enhancement. At large p_T the effect goes away as expected.

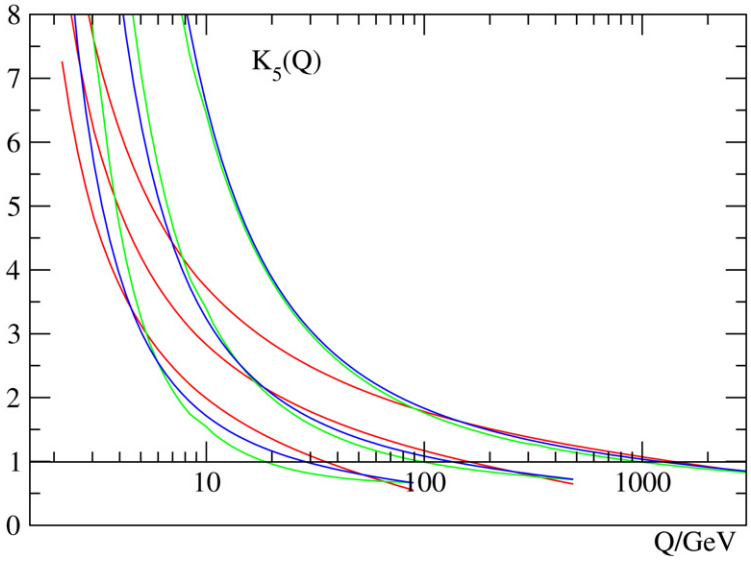

Fig. 21. The K-factor K_5, Eq. (4.20), appropriate for the gluonic contribution to Drell–Yan, vector boson production and prompt photon processes. The curves are labelled as in Fig. 17: blue is resummed, while red and green are estimates of fixed order perturbation theory at NLO and NNLO. (For interpretation of the references to colour in this figure legend, the reader is referred to the web version of this article.)

4.4. Drell–Yan and higher orders

Of course not all processes have the same structure of infrared singularities as heavy quark and inclusive jet production: as the number of particles in the final state increases, so does the range of possible infrared singularities. Indeed, adding one more particle to the final state generally adds one extra collinear and one extra soft singularity, thus increasing n in Eqs. (4.6) and (4.7) by two.

Consider for example the gluonic contribution to Drell–Yan or vector boson production, given by the diagrams in Fig. 3. The most singular of these diagrams is Fig. 3(c): there is a soft singularity from the timelike gluon, a collinear singularity from the splitting into a $q\bar{q}$ pair, and then further soft and collinear singularities from the final vector boson emission. Unless there are accidental cancellations, we thus expect the impact factor for this process to have a pole of order five at $M_1 + M_2 = 1$. The relevant K-factor is thus (using Eq. (4.7) with $n = 5$)

$$K_5(Q) = \frac{1}{L_z(\xi, t)} \int_{-i\infty}^{i\infty} \frac{dN}{2\pi i} e^{N\xi} \int_0^\infty d\tau\, \tau^4 e^{-\tau} L_z(N, t+\tau) \tag{4.20}$$

which may be evaluated by computing the τ integral numerically, just as we did for K_3 Eq. (4.9).

The results are shown in Fig. 21. Comparing K_5 to K_3 shown in Fig. 17, the extra soft and collinear singularities produce a further overall enhancement as expected. However the qualitative features of the two plots are very similar: in particular the resummed result starts to grow faster than the NLO result at about the same scale in each case. For W or Z production at LHC the correction is in the region of 20%–30%: it only becomes large at VLHC. However for pro-

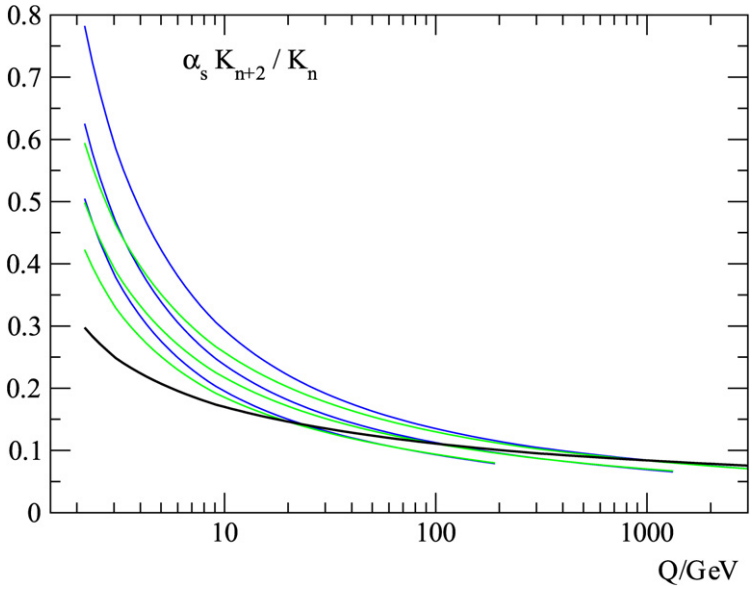

Fig. 22. The ratios $\alpha_s K_{n+2}/K_n$ for $n = 3$ (blue, upper) and $n = 5$ (green, lower) showing relative enhancement of subleading corrections. As usual the three curves of each colour are for Tevatron, LHC, and VLHC. Also shown is $\alpha_s(Q)$ (solid black) as a baseline expectation. (For interpretation of the references to colour in this figure legend, the reader is referred to the web version of this article.)

duction of Drell–Yan pairs at around 10 GeV at LHC the NLO correction is as large as a factor of three, and requires resummation.

For these gluon–gluon processes NLO means $O(\alpha\alpha_s^3)$, which is NNNLO in the usual nomenclature of fixed order perturbation theory. Thus unlike in the previous heavy quark and inclusive jet (i.e. $n = 3$) estimates, here even the NLO curve is a new result: only the LO contribution to the gluonic contribution to Drell–Yan and vector boson production, $gg \to W + X$ (i.e. the graphs in Fig. 3 but with the incoming gluons on-shell), has been computed exactly in fixed order perturbation theory [20].

We can also use Fig. 21 to estimate resummation corrections to prompt photon production, or to the three-jet inclusive cross-section, since the relevant diagrams again have the same structure as those in Fig. 3 (with for jets the quarks and vector bosons replaced by gluons) and thus the same structure of infrared singularities.

Since the number of infrared logarithms increases by two at each extra order in α_s, and since, unlike the logarithms from high energy ($N = 0$) and collinear ($M = 0$) singularities these logarithms are not being explicitly resummed, one might worry that they might destabilise the hierarchy of terms in the resummed perturbation theory [15]. To address this problem we note that we can estimate the size of subleading resummation corrections by computing the ratios $\alpha_s(Q)K_{n+2}(Q)/K_n(Q)$: these are plotted in Fig. 22 for $n = 3$ (heavy quark production and inclusive jets) and $n = 5$ (Drell–Yan and vector boson production). It is clear from this plot that even at low scales and at VLHC the enhancements due to the two extra infrared logarithms are never very substantial.

Moreover as n increases the enhancements are systematically reduced. The reason for this is not hard to find: a singularity of order n results in a smearing of the gluon–gluon luminosity with

a distribution proportional to $\tau^{n-1}e^{-\tau}$, Eq. (4.7), which is peaked at $\tau = n-1$. Since the scale dependence of the luminosity is very smooth, thanks to asymptotic freedom, the main effect of the smearing at large n is to shift the scale at which the luminosity is evaluated from t to $t+n-1$. Thus at large n

$$\frac{K_{n+2}(Q)}{K_n(Q)} \sim \frac{L_z(\xi, t+n+1)}{L_z(\xi, t+n-1)} \sim 1 + \frac{2}{L_z(\xi, t+n)} \frac{\partial}{\partial t} L_z(\xi, t+n), \tag{4.21}$$

which tends to one for large n and large t (see Fig. 14). It follows that there is no reason to suspect that the infrared logarithms spoil our resummed perturbation theory: for high energy processes with a single hard scale, we have indeed resummed all large logarithms.

5. Rapidity distributions

5.1. Gluon–gluon rapidity

Besides hadroproduction total cross-sections it is also interesting to consider rapidity distributions: in the central rapidity region both partons carry roughly the same fraction of longitudinal momentum, but at large rapidities one of the partons is at a much smaller value of x than the other (see Fig. 1 for the ranges covered at various machines) so it is perhaps here that one might expect the effects of resummation to be most significant.

We define

$$z \equiv x_1 x_2, \qquad \eta = \frac{1}{2}\ln(x_1/x_2), \tag{5.1}$$

so that $s = zS$ is the centre-of-mass energy in the partonic collision, and η is the (pseudo)-rapidity: $\eta = 0$ in the central region, becoming large and positive/negative in the forward/backward regions. In terms of z and η the fraction of longitudinal momentum in each of the two colliding partons is

$$x_1 = \sqrt{z}e^{\eta}, \qquad x_2 = \sqrt{z}e^{-\eta}. \tag{5.2}$$

Since $s \geqslant Q^2$, while $x_1, x_2 \leqslant 1$, we must have

$$\rho \leqslant z \leqslant 1, \qquad \frac{1}{2}\ln z \leqslant \eta \leqslant \frac{1}{2}\ln\frac{1}{z}. \tag{5.3}$$

In terms of z and η the factorization formula (2.2) may be written

$$\Sigma_{hh}(\rho, Q) = \int_\rho^1 \frac{dz}{z} \int_{\frac{1}{2}\ln z}^{\frac{1}{2}\ln\frac{1}{z}} d\eta \int \frac{d^2\mathbf{k}_1}{\pi\mathbf{k}_1^2} \int \frac{d^2\mathbf{k}_2}{\pi\mathbf{k}_1^2} \times \Sigma_{gg}\left(\frac{\rho}{z}, \frac{\mathbf{k}_1}{Q}, \frac{\mathbf{k}_2}{Q}\right) G\left(\sqrt{z}e^{\eta}, \mathbf{k}_1^2\right) G\left(\sqrt{z}e^{-\eta}, \mathbf{k}_2^2\right). \tag{5.4}$$

Since the hard cross-section depends only on z, not on η (because of invariance under longitudinal boosts), we may perform the integral over η first to give the gluon–gluon luminosity (4.1). If instead however we perform the integrals in the opposite order

$$\int_\rho^1 \frac{dz}{z} \int_{\frac{1}{2}\ln z}^{\frac{1}{2}\ln\frac{1}{z}} d\eta = \int_{-\xi/2}^{\xi/2} d\eta \int_\rho^{e^{-2|\eta|}} \frac{dz}{z}, \tag{5.5}$$

where as usual $\xi = \ln 1/\rho$, the factorization (5.4) may be written instead as a factorization for the differential cross-section:

$$\frac{d\Sigma_{hh}}{d\eta} = \int_{\rho}^{e^{-2|\eta|}} \frac{dz}{z} \int \frac{d^2\mathbf{k}_1}{\pi \mathbf{k}_1^2} \int \frac{d^2\mathbf{k}_2}{\pi \mathbf{k}_2^2} \Sigma_{gg}\left(\frac{\rho}{z}, \frac{\mathbf{k}_1}{Q}, \frac{\mathbf{k}_2}{Q}\right) G\left(\sqrt{z}e^{\eta}, \mathbf{k}_1^2\right) G\left(\sqrt{z}e^{-\eta}, \mathbf{k}_2^2\right). \tag{5.6}$$

At high energy the explicit dependence of the hard cross-section $\Sigma_{gg}(\frac{\rho}{z}, \frac{\mathbf{k}_1}{Q}, \frac{\mathbf{k}_2}{Q})$ on z is relatively weak: the dominant contribution to the z dependence of the collinear cross-section comes about through the dependence of the off-shell cross-section on the transverse momenta. This makes the computation of rapidity distributions at high energy particularly simple, since the rapidities of the final state particles are directly related to the rapidities of the colliding partons. It is then useful to define gluon–gluon rapidity distribution

$$L_\eta\left(\eta, k_1^2, k_2^2, \rho\right) = \int_{\rho}^{e^{-2|\eta|}} \frac{dz}{z} G\left(\sqrt{z}e^{\eta}, k_1^2\right) G\left(\sqrt{z}e^{-\eta}, k_2^2\right). \tag{5.7}$$

Clearly the normalization of this distribution is not independent of that of the gluon–gluon luminosity (4.1): in fact

$$\int_{-\xi/2}^{\xi/2} d\eta\, L_\eta\left(\eta, k_1^2, k_2^2, \rho\right) = \int_{\rho}^{1} \frac{dz}{z} L_z\left(z, k_1^2, k_2^2\right). \tag{5.8}$$

Again the gluon–gluon rapidity distribution may be readily computed from $G(x, Q)$ displayed in Fig. 4: the result for $L_\eta(\eta, Q) \equiv L_\eta(\eta, Q^2, Q^2, \rho)$ is shown in Fig. 23 for both B-production and W-production at LHC. The falloff as $\eta \to \pm\xi/2$ is very rapid, essentially because the gluon is very small at large x (remember that in all these calculation we are suppressing the quark contribution, so the valence region is underpopulated).

In terms of the gluon–gluon rapidity at high energy the differential cross-section is then given by

$$\begin{aligned}\frac{d\Sigma_{hh}}{d\eta} &\simeq \int \frac{d^2\mathbf{k}_1}{\pi \mathbf{k}_1^2} \int \frac{d^2\mathbf{k}_2}{\pi \mathbf{k}_2^2} \Sigma_{gg}\left(1, \frac{\mathbf{k}_1}{Q}, \frac{\mathbf{k}_2}{Q}\right) L_\eta\left(\eta, k_1^2, k_2^2, \rho\right) \\ &= \int_{-i\infty}^{i\infty} \frac{dM_1}{2\pi i} \frac{dM_2}{2\pi i} e^{t(M_1+M_2)} H(0, M_1, M_2) L_\eta(\eta, M_1, M_2, \rho),\end{aligned} \tag{5.9}$$

where the (double) Mellin transform is defined in the usual way:

$$L_\eta(\eta, M_1, M_2, \rho) \equiv \int_0^{\infty} \frac{dk_1^2}{k_1^2} \left(\frac{k_1^2}{\Lambda^2}\right)^{-M_1} \int_0^{\infty} \frac{dk_2^2}{k_2^2} \left(\frac{k_2^2}{\Lambda^2}\right)^{-M_2} L_\eta(\eta, k_1, k_2, \rho). \tag{5.10}$$

Note that unlike (4.3) the expression (5.9) only holds in the approximation where we ignore the N dependence in the hard cross-section $H(N, M_1, M_2)$.

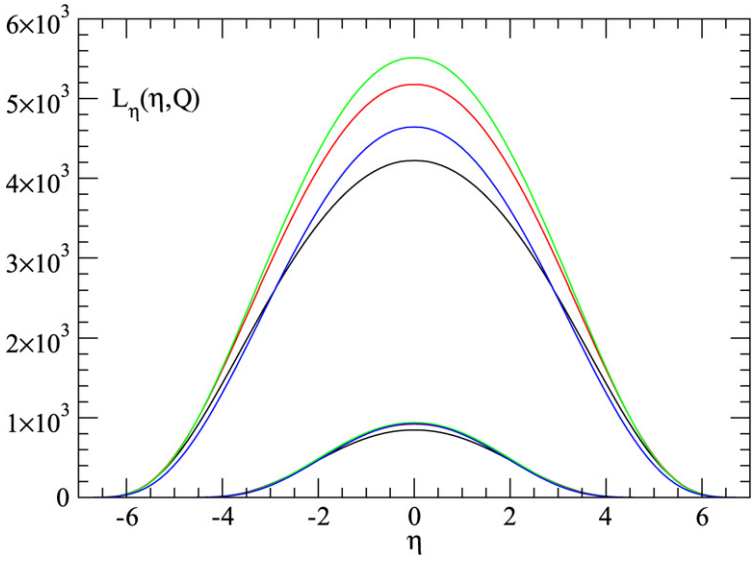

Fig. 23. The gluon–gluon rapidity distribution $L_\eta(\eta, Q)$ at the LHC for B-production ($Q = 10$ GeV) (upper curves) and W-production ($Q = 75$ GeV) (lower curves). The blue curves are for gluons evolved using NLO resummation, while the black, red and green curves are for gluons evolved using LO, NLO and NNLO GLAP. (For interpretation of the references to colour in this figure legend, the reader is referred to the web version of this article.)

5.2. *B-production and W-production at LHC*

For a particular impact factor $H(0, M_1, M_2)$ the corresponding differential cross-section (5.9) may be readily evaluated using Eqs. (4.5) for powers of M_1 and M_2, and the exponentiation trick Eq. (4.6) for singularities. We consider two examples: B-production at the LHC, for which we use the impact factor (4.13) expanded as (4.16) or (4.17), and the gluon–gluon contribution to W-production at LHC, which we assume is dominated at high energy by the infrared singularities in final state emission (Fig. 3(c)), and may thus be modelled by an $n = 5$ pole:

$$\begin{aligned}\frac{d\Sigma^W_{hh}}{d\eta} &\simeq \alpha\alpha_s^2 \int_{-i\infty}^{i\infty} \frac{dM_1}{2\pi i}\frac{dM_2}{2\pi i} e^{t(M_1+M_2)} \frac{r}{(1-M_2-M_2)^5} L_\eta(\eta, M_1, M_2, \rho)\Big|_{Q=m_W} \\ &= \alpha\alpha_s^2 r \int_0^\infty d\tau\, \tau^4 e^{-\tau} L_\eta(\eta, t+\tau)\Big|_{t=\ln m_W^2/\Lambda^2}, \end{aligned} \tag{5.11}$$

where r is a normalization factor (just a number), and in the second line we have used Eq. (4.20) to evaluate the integrals over M_1 and M_2 just as we did in Eq. (4.6). For B-production we use a similar expression, but here of course we take $n = 3$. Note however that now the integration over z in Eq. (5.7) can take us into the region of large x_1 or x_2 at high rapidities, so here we must take care to match the cross-section smoothly in this region to the fixed order calculation to avoid spurious contributions.

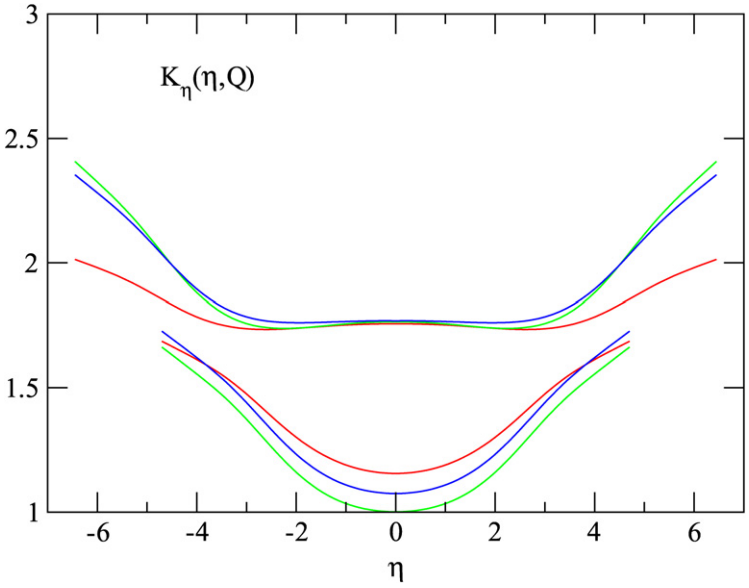

Fig. 24. The K-factors $K_\eta(\eta, m_B)$ (upper curves) $K_\eta(\eta, m_W)$ (lower curves) for the rapidity distribution of B-production and (the gluon–gluon component of) W-production at the LHC. As in Figs. 17 and 19 the blue curves are the resummed result, while the red and green curves are NLO and NNLO perturbation theory, estimated in the usual way. (For interpretation of the references to colour in this figure legend, the reader is referred to the web version of this article.)

Again we express the results of these calculations as K-factors: here

$$K_\eta(\eta, m_W) = \frac{d\Sigma^W_{hh}}{d\eta} \Big/ \frac{d\Sigma^0_{hh}}{d\eta}\bigg|_{Q=m_W}, \tag{5.12}$$

and a similar expression for $K^B_\eta(\eta, m_B)$. The denominator is in each case the result obtained by setting $M_1 = M_2 = 0$ in the impact factor, and thus divides out the unknown normalization r and the primary dependence on the gluon–gluon rapidity. The corresponding K-factors in perturbation theory may be estimated by expansion in powers of M_1 and M_2, and using the appropriate GLAP evolved gluon–gluon rapidity distribution.

The results of these calculations are shown in Fig. 24. For B-production the K-factor is already substantial in the central rapidity region, and rises further at large rapidities where one of x_1 or x_2 becomes very small. This rise is rather steeper for the resummed and NNLO calculations than it is at NLO, as expected. However this prediction needs to be interpreted with care, since at large rapidities one of the gluons is moving towards the high x region, which is poorly modelled in this calculation since there are no quark contributions. For the gluon–gluon contribution to W production the K-factors in the central region are all rather small, but increase quite quickly with rapidity. However here the resummed calculation is close to the NLO and NNLO calculations throughout the whole range. Note again that here even the NLO curve is a new result. The change in the shape of the rapidity distribution due to what is formally a NNNLO (i.e. $O(\alpha\alpha_s^3)$) contribution is thus quite striking.

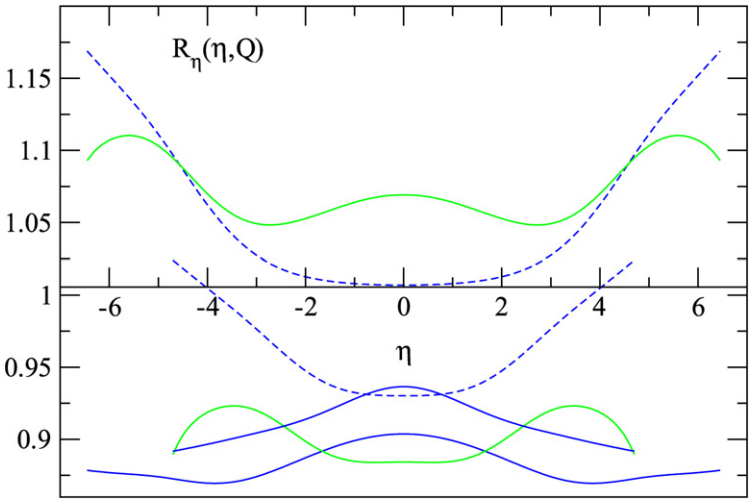

Fig. 25. The resummation factor R_η for B-production (outer curves) and W-production (inner curves) at the LHC plotted against the rapidity η. The solid blue (lower) curves correspond to fully resummed calculations, while the dashed curves are the same calculations but with the effect of the evolution on the gluon–gluon rapidity distribution factored out. The true size of the resummation effect probably lies somewhere between these two extremes. The green (upper) curves are the result of a NNLO fixed order calculation. (For interpretation of the references to colour in this figure legend, the reader is referred to the web version of this article.)

To see more clearly the effect of the resummation alone, we also compute the "resummation factor"

$$R_\eta(\eta, m_W) = \frac{d\Sigma_{hh}^W}{d\eta} \Big/ \left.\frac{d\Sigma_{hh}^{\rm NLO}}{d\eta}\right|_{Q=m_W}, \tag{5.13}$$

again with a similarly expression for B-production, where now the reference differential cross-section is the NLO fixed order cross-section computed with a NLO GLAP evolved rapidity distribution, so that the effect of the resummation in both evolution and partonic cross-section are combined. The results are shown in Fig. 25. Resummation reduces the B cross-section by around 10% across the whole rapidity region, this effect being due almost entirely to evolution since without it there is an enhancement rising to around 15% at large rapidity. The effect of resummation on W-production is rather less pronounced. Note that in both cases the enhancement due to the infrared singularities in the hard cross-section is largely cancelled by the suppression of the luminosity, leaving a relatively flat distribution.

6. Conclusions

We have shown that the problem of integration of infrared singularities in photoproduction, electroproduction and hadroproduction cross-sections due to final state gluons becoming soft or collinear [15,16] may be solved through an exponentiation trick Eqs. (3.11) and (4.6) respectively. This enables us to show that despite the dramatic enhancements found when the coupling is fixed, when the coupling runs the effects are much more modest. In particular we have shown that when the coupling runs the growth of the inclusive cross-sections at asymptotically high energy is given universally by the growth of the resummed integrated gluon distribution, with

no process dependent power enhancements: all the infrared singularities are correctly factorised into the initial non-perturbative distribution, as they should be.

We find furthermore that except at very low scales the inclusive cross-sections are well approximated by keeping only the first few terms in the Taylor expansion of the partonic cross-section in powers of M, irrespective of the presence of the nearby infrared singularities. Since this expansion in powers of M is closely related to the usual perturbative expansion of the hard cross-section in powers of α_s/N, this enables us to understand the behaviour of the expansion to fixed orders in α_s. In particular we have shown that the large K-factors commonly found in hadroproduction processes at NLO and NNLO are at high energy due mainly to the infrared final state singularities (compare Figs. 16, 17, 19, 21 and 24), and moreover that although in some kinematic regions (high energy, low invariant mass and large rapidity) the NNLO correction to the hard cross-section may be important, the series converges sufficiently rapidly that NNNLO corrections are in practice usually small. This is reassuring.

We also find that although in the resummed perturbation theory the number of infrared logarithms increases by two for every extra power of α_s, the effect of the extra logarithms is sufficiently benign that the hierarchy of the resummed perturbative expansion is not spoiled, and thus no further resummation is necessary. This again is due to asymptotic freedom, in the sense that it is only true when the coupling runs.

A useful way to characterise this interplay between collinear and high energy resummation is to ask in which regions of the kinematic plane Fig. 1 logarithms of Q^2 or logarithms of x are more important. If the former are dominant, we may expand the partonic cross-section $H(N, M_1, M_2)$ in powers of M_1 and M_2, keeping the full dependence on N, while if the small x logarithms dominate, we may expand in powers of N but keeping the full dependence on M_1 and M_2. The relevant regions are thus characterised by the relative importance of factors of M and factors of N, or more specifically of the two integrals

$$\begin{aligned}
\dot{L}_z(\xi,t) &\equiv \int_{-i\infty}^{i\infty}\frac{dN}{2\pi i}e^{\xi N}\int_{-i\infty}^{i\infty}\frac{dM_1}{2\pi i}\frac{dM_2}{2\pi i}e^{t(M_1+M_2)}(M_1+M_2)L_z(N,M_1,M_2)\\
&= \frac{\partial}{\partial t}L_z(\rho,t),\\
L'_z(\xi,t) &\equiv \int_{-i\infty}^{i\infty}\frac{dN}{2\pi i}e^{\xi N}\int_{-i\infty}^{i\infty}\frac{dM_1}{2\pi i}\frac{dM_2}{2\pi i}e^{t(M_1+M_2)}NL_z(N,M_1,M_2)\\
&= \frac{\partial}{\partial \xi}L_z(\rho,t).
\end{aligned}\tag{6.1}$$

These integrals may be computed for the gluon–gluon luminosity shown in Fig. 12: the results are displayed in Fig. 1. Clearly when $L'_z \gg \dot{L}_z$, high energy logarithms are relatively unimportant and the usual on-shell perturbative approximation to the hard cross-section is applicable. However when $L'_z \ll \dot{L}_z$, the high energy logarithms are the most important, and we should use the off-shell perturbative expansion of the hard cross-section, perhaps with $N=0$. It can be seen from Fig. 1 that this is only true at very low scales, close to the initial boundary condition. More interesting is the intermediate region $L'_z \sim \dot{L}_z$, in which resummation of both types of logarithm is necessary, and in which we may usefully expand both in N and in M. This region is important not only at high rapidity, but also in the central region when the invariant mass of the produced particles is not too high.

The reason that the region dominated by logarithms of Q^2 is so much larger than that dominated by logarithms of x is very simple: when the coupling runs with Q^2 the variation of the luminosity with $t = \ln Q^2$ is much weaker than its variation with $\xi = \ln S/Q^2$, so factors of M are less significant than factors of N. This observation underpins the success of fixed order perturbation theory (which amounts to expansion in powers of M) in computing hard cross-sections in kinematic regions where one might naively have expected it to fail due to unresummed logarithms of x.

We have shown a variety of estimates of the size of the high energy resummation effects compared to standard NLO perturbation theory. Our basic conclusion is that the effect of resummation in the partonic cross-section is an enhancement similar in size to that of a perturbative NNLO correction, while in the full cross-section the resummation of the gluon distribution produces an effect of similar magnitude but opposite sign. The net result is thus rather less than might be expected from NNLO considerations alone, since there is substantial cancellation. In fact we find that for a wide range of processes, each over a wide kinematic range, the net effect of resummation seems to be a suppression of between 5% and 10% (compare the blue curves in Figs. 11, 18, 20 and 25). This seems to suggest that the hard scale Q may not be the optimal factorisation scale for high energy processes.

However it must also be remembered that the suppression of the gluon due to resummed evolution is probably being overestimated in these calculations, since the initial distribution at 2 GeV is kept fixed, rather than fitted to data (see for example the resummed fits in Refs. [26,38,39]). The true band of current uncertainty thus probably lies between these two extremes, i.e. between the solid and dashed blue curves in the figures. Thus for example in the total cross-section for hadronic B-production (Fig. 20) the resummation corrections are as small as $-5 \pm 5\%$ at the Tevatron, rising to $5 \pm 10\%$ at the LHC and $20 \pm 20\%$ at a VLHC. These figures are still rather lower than suggested by the leading order calculations in Ref. [14] and substantially smaller than the fixed coupling estimates in [15,16]. The effects on rapidity distributions may be rather larger, particularly at large rapidities: for B production at LHC resummation effects might be as large as $\pm 15\%$ at rapidities of 5 or so. Similar estimates should hold for inclusive jet cross-sections.

For the gluonic contribution to Drell–Yan at LHC the effects are a little larger, since the infrared singularity is stronger. However for vector boson production the corrections are still modest since the hard scale is relatively large, though they are even so comparable to other sources of uncertainty. The predicted enhancement at large rapidities shown in Fig. 24 is particularly striking.

Refining these estimates into precise predictions is now straightforward: there are no longer any theoretical obstacles to computing cross-sections for hadroproduction processes correct to NLO which simultaneously resum all leading and next-to-leading logarithms of S and Q^2. However there is still a lot of work to be done.

Firstly it would be useful to have complete calculations of off-shell partonic cross-sections for a wider variety of hadronic processes: at the moment all we have are cross-sections for heavy quark production [16,27] and Higgs production in the $m_t \to \infty$ limit [17]. The key partonic calculation for the future is clearly Drell–Yan and vector-boson production, both to confirm the conjectured structure of infrared singularities and provide a firm prediction for these benchmark processes. As explained above, it is important to match these cross-sections to the standard perturbative (on-shell) cross-sections, preferably by keeping the full N dependence when going off-shell. However for most purposes it is probably sufficient to treat the off-shellness perturba-

tively, keeping only the first few powers of M. The off-shell calculations are then complementary to the more usual fixed order (on-shell) calculations, offering a short cut to new results.

Secondly, for more precise calculations we clearly need to include quark effects, particularly in the high rapidity region where one of the partons is in the valence region. Including quarks in the resummed singlet evolution is no longer a problem [40], and including the contribution of initial state quarks to the resummed partonic cross-sections is also well understood [2,16,26].

Finally, for accurate resummed predictions it is necessary to produce resummed parton densities, fitted to data using resummed theoretical predictions. Previous experience [26,38] suggests that much of the effect of resummation in the evolution might then be absorbed into the parton distributions, so without this ingredient resummation effects in the parton distribution functions are probably being overestimated. In order to obtain unbiased resummed parton distributions with sensible experimental uncertainty distributions, it will be necessary to use a statistical approach such as that currently being developed by the NNPDF Collaboration [41].

Acknowledgements

I would like to thank M. Ciafaloni for emphasising to me long ago the importance of going beyond the saddle point approximation when the coupling runs, R.K. Ellis for encouraging me to persevere with the hadronic singularity problem, L. Magnea and G. Sterman for encouraging me to write it up, R.K. Ellis and S. Forte for comments on the completed manuscript, and finally an anonymous referee for several constructive remarks on the nature of the infrared singularities. This work was done in the context of the Scottish Universities Physics Alliance.

References

[1] S. Catani, F. Fiorani, G. Marchesini, Nucl. Phys. B 336 (1990) 18;
S. Catani, et al., Nucl. Phys. B 361 (1991) 645.
[2] S. Catani, F. Hautmann, Phys. Lett. B 315 (1993) 157;
S. Catani, F. Hautmann, Nucl. Phys. B 427 (1994) 475.
[3] V.S. Fadin, L.N. Lipatov, Phys. Lett. B 429 (1998) 127;
V.S. Fadin, et al., Phys. Lett. B 359 (1995) 181;
V.S. Fadin, et al., Phys. Lett. B 387 (1996) 593;
V.S. Fadin, et al., Nucl. Phys. B 406 (1993) 259;
V.S. Fadin, et al., Phys. Rev. D 50 (1994) 5893;
V.S. Fadin, et al., Phys. Lett. B 389 (1996) 737;
V.S. Fadin, et al., Nucl. Phys. B 477 (1996) 767;
V.S. Fadin, et al., Phys. Lett. B 415 (1997) 97;
V.S. Fadin, et al., Phys. Lett. B 422 (1998) 287.
[4] G. Camici, M. Ciafaloni, Phys. Lett. B 412 (1997) 396;
G. Camici, M. Ciafaloni, Phys. Lett. B 430 (1998) 349.
[5] V. del Duca, Phys. Rev. D 54 (1996) 989;
V. del Duca, Phys. Rev. D 54 (1996) 4474;
V. del Duca, C.R. Schmidt, Phys. Rev. D 57 (1998) 4069;
Z. Bern, V. del Duca, C.R. Schmidt, Phys. Lett. B 445 (1998) 168.
[6] R.D. Ball, S. Forte, hep-ph/9805315.
[7] G. Salam, JHEP 9807 (1998) 19;
M. Ciafaloni, D. Colferai, G.P. Salam, JHEP 9910 (1999) 17.
[8] R.D. Ball, S. Forte, Phys. Lett. B 405 (1997) 317.
[9] G. Altarelli, R.D. Ball, S. Forte, Nucl. Phys. B 575 (2000) 313.
[10] M. Ciafaloni, M. Taiuti, A.H. Mueller, Nucl. Phys. B 616 (2001) 349;
M. Ciafaloni, et al., Phys. Rev. D 66 (2002) 054014.

[11] G. Altarelli, R.D. Ball, S. Forte, Nucl. Phys. B 621 (2002) 359;
G. Altarelli, R.D. Ball, S. Forte, Nucl. Phys. B 674 (2003) 459.
[12] G. Altarelli, R.D. Ball, S. Forte, Nucl. Phys. B 742 (2006) 1.
[13] M. Ciafaloni, et al., Phys. Rev. D 68 (2003) 114003;
M. Ciafaloni, et al., Phys. Lett. B 635 (2006) 320.
[14] J.C. Collins, R.K. Ellis, Nucl. Phys. B 360 (1991) 3.
[15] S. Catani, M. Ciafaloni, F. Hautmann, Phys. Lett. B 242 (1990) 97;
S. Catani, M. Ciafaloni, F. Hautmann, Nucl. Phys. B 366 (1991) 135.
[16] R.D. Ball, R.K. Ellis, JHEP 0105 (2001) 053.
[17] F. Hautmann, Phys. Lett. B 535 (2002) 159;
A.V. Lipatov, N.P. Zotov, Eur. Phys. J. C 44 (2005) 559.
[18] A. De Rújula, et al., Phys. Rev. D 10 (1974) 1649.
[19] R.D. Ball, S. Forte, Phys. Lett. B 335 (1994) 77;
R.D. Ball, S. Forte, Phys. Lett. B 336 (1994) 77;
R.D. Ball, S. Forte, Acta Phys. Pol. B 26 (1995) 2097.
[20] R. Hamberg, W.L. van Neerven, T. Matsuura, Nucl. Phys. B 359 (1991) 343;
R. Hamberg, W.L. van Neerven, T. Matsuura, Nucl. Phys. B 644 (2002) 403, Erratum.
[21] L.N. Lipatov, Sov. Phys. JETP 63 (1986) 5.
[22] R.D. Ball, S. Forte, Nucl. Phys. B 742 (2006) 158.
[23] S. Marzani, R.D. Ball, P. Falgari, S. Forte, arXiv: 0704.2404 [hep-ph].
[24] T. Jaroszewicz, Phys. Lett. B 116 (1982) 291.
[25] R.D. Ball, S. Forte, Phys. Lett. B 351 (1995) 313;
R.D. Ball, S. Forte, Phys. Lett. B 359 (1995) 362;
R.K. Ellis, F. Hautmann, B.R. Webber, Phys. Lett. B 348 (1995) 582.
[26] G. Altarelli, R.D. Ball, S. Forte, Nucl. Phys. B 599 (2001) 383;
See also G. Altarelli, R.D. Ball, S. Forte, hep-ph/0104246.
[27] G. Camici, M. Ciafaloni, Nucl. Phys. B 496 (1997) 305;
G. Camici, M. Ciafaloni, Nucl. Phys. B 607 (2001) 431, Erratum.
[28] R.D. Ball, S. Forte, Phys. Lett. B 465 (1999) 271.
[29] M. Ciafaloni, Phys. Lett. B 356 (1995) 74.
[30] M. Ciafaloni, D. Colferai, G.P. Salam, JHEP 0007 (2000) 054.
[31] M. Ciafaloni, D. Colferai, JHEP 0509 (2005) 069.
[32] J.C. Collins, J. Kwiecinski, Nucl. Phys. B 316 (1989) 307;
Y.V. Kovchegov, A.H. Mueller, Phys. Lett. B 439 (1998) 428;
N. Arnesto, J. Bartels, M.A. Braun, Phys. Lett. B 442 (1998) 459.
[33] R.S. Thorne, Phys. Lett. B 474 (2000) 372;
R.S. Thorne, Phys. Rev. D 64 (2001) 074005.
[34] J.S. Schwinger, Phys. Rev. 82 (1951) 664.
[35] S. Catani, M. Ciafaloni, F. Hautmann, DESY HERA Workshop 1991, 690-711.
[36] R.K. Ellis, D.A. Ross, Nucl. Phys. B 345 (1990) 79.
[37] R.K. Ellis, P. Nason, Nucl. Phys. B 312 (1989) 551.
[38] R.D. Ball, S. Forte, Phys. Lett. B 358 (1995) 365.
[39] C.D. White, R.S. Thorne, Phys. Rev. D 75 (2007) 034005.
[40] G. Altarelli, R.D. Ball, S. Forte, in preparation.
[41] L. Del Debbio, et al., NNPDF Collaboration, JHEP 0703 (2007) 039;
J. Rojo, et al., NNPDF Collaboration, arXiv: 0706.2130 [hep-ph].